Faculty of Graduate Studies

Novel synthesis of Pencil Graphite -supported Nano-Scale Zero valent Iron for removal of Diclofenac Sodium in aqueous solutions

تواليف جديد باستخدام جسيمات الحديد النانوية صفرية التكافؤ المدعمة بجرافيت قلم الرصاص لإزالة ديكلوفيناك الصوديوم من المحاليل المائية

This thesis was submitted in partial fulfillment of the requirements for the

Master's Degree in Applied Chemistry

From the Faculty of Graduate Studies at Birzeit University, Palestine.

Leena AL Rimawi

1185237

Supervisors:

Dr. Mohammed Al-jabarei & Dr. Saleh Sulaiman

2022

Novel synthesis of Pencil Graphite -supported Nano-Scale Zero valent Iron for removal of Diclofenac Sodium in aqueous solutions

By

Leena AL Rimawi

This thesis was defended successfully on 30 /03/2022 and approved by:

Committee Members	Signature
Dr. Mohammed Al-jabarei Supervisor Chemistry Department-Faculty Member Birzeit University	_____
Dr. Saleh Sulaiman Supervisor Chemistry Department-Faculty Member Birzeit University	_____
Prof. Talal Shahwan Committee Member Chemistry Department-Faculty Member Birzeit University	_____
Dr. Mazen Nazal Committee Member Center for Environment and Water, Research Institute King Fahd University	

Acknowledgment

First, I am very grateful to God for being with me and helping me to complete this thesis. I would like to thank my supervisor's Dr. Mohammed Al-jabarei and Dr.Saleh Sulaiman for supporting me with valuable advice and their efforts, comments, and motivation to complete this work.

I would also like to thank Dr.Talal Sahwan and Dr. Mazen Nazal for their valuable comments and support and their time in reading and assessing the thesis.

I would like to thank the chemistry department members at Birzeit University, and lab technicians: Mr. Asem Mubarak, Mr. Azmi Dudin, and Dr. Ibrahim Shalash for their help throughout my thesis experiments.

Finally, a deep thanks to my family for their support and encouragement. And a special thanks to my mother for her help and care.

Table of contents

List of Figures

List of Tables

Abbreviations

AC	Activated Carbon
BET	Brunauer, Emmett and Teller
DCF	Diclofenac Sodium
EDS	Energy-Dispersive Spectroscopy
FE-TEM	Field Emission Transmittance Electron Microscope
FT-IR	Fourier Transform- Infrared Spectroscopy
NP	Nanoparticle
NSAID	non-steroidal anti-inflammatory drug
nZVI	Nano Zero Valent Iron
OAC	Oxidized Activated Carbon
PG	Pencil Graphite
PZC	The point of zero charge
rGO	reduced Graphene Oxide
SEM-EDX	Scanning Electron Microscope coupled with Energy Dispersive X-ray
TEM	Transmission Electron Microscopy
UV-vis	Ultra Violet- visible spectroscopy
XRD	X-Ray Diffraction

Abstract

Removal of water contaminations is the major concern in the recent decade, the pharmaceutical compounds are one of the main water pollutants in the sewage of human activity. The fate of Pharmaceutical compounds in an aquatic environment is highly concerned. Diclofenac Sodium (DCF) is a nonsteroidal anti-inflammatory drug, analgesic, and antipyretic, considered as the most common drug found to accumulate in environmental compartments.

Nano zero-valent iron (nZVI) and a new composite adsorbent (nZVI -PG) were synthesized and characterized using Fourier Transform- Infrared Spectroscopy (FT-IR), X-Ray Diffraction (XRD), Transmission Electron Microscopy (TEM), and Energy-dispersive spectroscopy (EDS) techniques.

The comparative study between nZVI and nZVI –PG composite was performed to evaluate the effectiveness of PG as a supporter matrix for nZVI for removal of DCF from aqueous solution. The presence of the adsorbate compound on the surface of the particles was being investigated by FT-IR and UV-vis. Thermodynamic and kinetic parameters were studied over different conditions of concentrations, contact time, nZVI dose, pH, and temperature.

The results showed that the DCF removal efficiency using nZVI -PG composite is higher than that of nZVI using the same amount of adsorbent (Fe^0). The kinetic models, which were used to explain the adsorption process and the kinetic results showed that DCF adsorption using nZVI and nZVI -PG composite have followed the pseudo-second-order model. The equilibrium experimental data were analyzed using Langmuir and Freundlich isotherm models at 298 K, and the isotherm studies showed that the maximum adsorption capacity of the nZVI -PG composite was higher than nZVI. The thermodynamic parameters indicated that the adsorption of DCF via both types of adsorbent is endothermic in nature.

The developed composite may be useful for the removal of DCF drug residue from natural water resources at nutral pH values with high efficiency.

الملخص باللغة العربية

لقد أصبح الحصول على مياه نقية خالية من الملوثات أهم ما يشغل الانسان في الوقت الحاضر. يعود ذلك الى الضغط الحاصل على مصادر المياه نتيجة للتطور الصناعي والنمو السكاني. صعوبة التخلص من هذه الملوثات وعلى رأسها بقايا المركبات الدوائية وتراكمها في مصادر المياه بعد وصولها عبر المياه العادمة أصبحت مشكلة يسعى الباحثيين الى إيجاد الحلول المناسبة لازالتها نظرا لخطورتها على البيئة والانسان. من المركبات الدوائية التي وجدت بتراكيز عالية في مياه الصرف الصحي والمعروفة بمقاومتها للتحلل البيولوجي ديكلوفيناك الصوديوم (DCF) وهو عقار مضاد للالتهابات ومسكن للألام وخافض للحرارة ، ويعتبر من أكثر المركبات الدوائية شيوعًا نتيجة لكثرة إستخدامه. حديثا إكتسبت تقنيات النانو أهمية كبيرة لمساهمتها في حل هذه المشكلة. في هذه الدراسة تم تصنيع جسيمات الحديد النانوية nZVI وجسيمات جديدة من المركبات (nZVI -PG) وتوصيفهما باستخدام تقنيات (FT-IR) و (XRD) و (TEM)و(EDS). تم إجراء دراسة مقارنة بين مركب nZVI -PG و nZVI لتقييم فعالية PG كمصفوفة داعمة ل nZVI لإزالة DCF من المحلول المائي. تم فحص خصائص الجسيمات التي تم تحضيرها وادمصاص المركب على سطحها بواسطة FT-IR وUV-Vis .

تمت دراسة معلومات الديناميكيا الحرارية والحركية على ظروف مختلفة من التركيزات ووقت التلامس وجرعة nZVI ودرجة الحموضة ودرجة الحرارة. أظهرت النتائج أن عملية إزالة DCF باستخدام جسيمات nZVI -PG كانت أعلى من تلك الخاصة بـجسيماتnZVI باستخدام تفس الكمية من جسيمات (Fe^0). أظهرت النماذج الحركية ، التي استخدمت لشرح عملية الامتزاز والنتائج الحركية ، أن امتزاز DCFباستخدام مركبات نانوية nZVI و nZVI -PG قد اتبعت نموذج معادلة الدرجة الثانية .

تم تحليل البيانات التجريبية للتوازن باستخدام نموذجي متساوي الحرارة Langmuir و Freundlich عند درجة حرارة 298 كلفن ، وتظهر دراسات متساوي الحرارة أن السعة القصوى لامتصاص مركب -nZVI

PG أعلى من nZVI. أشارت النتائج الديناميكية الحرارية إلى أن امتصاص DCF عبر كلا النوعين من الممتزات هو طبيعة ماصة للحرارة. الجسيمات المطورة قد تكون مفيدة لإزالة بقايا دواء DCF من موارد المياه الطبيعية عند درجات حموضة عادية بكميات صغيرة من الممتزات.

1. Introduction

1.1 Water pollution and pharmaceuticals

The revolution industry and rapid growth of population make water pollution a global problem and effect on the environment and human beings,[1-2] leads to many infectious diseases, that affect human health causing illness, such as typhoid fever, diarrhea, vomiting, and kidney problem.[3-4]

Organic contaminants like surfactants, pesticides, fertilizers, plastics, polythene bags, pharmaceuticals, and other chemicals reach environmental water resources causing water pollution, which is dangerous to human health.[5]

Also, the continuous production and development of new chemicals without having information about their impact on the environment may contribute to the increasing environmental pollution. So, more organic contaminants have been detected in wastewater, which could affect the surface and groundwater.[6]

Pharmaceutical compounds are one of the most significant pollutants in wastewater, that are produced and used in large quantities which lead to the uncontrolled continuous release of these contaminants to the water environment. Therefore, increase the concern of aquatic environment due to their biological activity and toxicity for human and water organisms.[7]

Pharmaceutical compounds have been found in large quantity in sewage treatment plant effluents and surface waters, and less abundant in drinking water and groundwater.[8]

The high concentration of the active pharmaceutical compounds in water, which ranged from ng/L to μg/L, attracts researchers attention to investigate the fate and occurrence of such compounds in the aquatic environment.[9-10]

Consuming drugs can easily move to the environment compartment due to their Low volatility, upraised polarity, and partial metabolization. Pharmaceutical compounds in the aquatic environment are classified into beta-blockers, hormones, antibiotics, anti-inflammatory, and analgesics.[11]

Pharmaceutical compounds enter the surface and groundwater through effluent discharge, resulting in the movement of pharmaceutical pollutants to sewage sludge by the sorption process that occurs during the treatment in Waste Water Treatment Plants. The continuous infusion of pharmaceutical effluents from Waste Water Treatment Plants is considered one of the persistent pollutants in the aqueous environment.[12-13]

Anti-inflammatory drugs are one of the widespread drugs used for the relief of pain, inflammation, and fever. But they are the most resistant compounds in wastewater treatment effluents, that have adverse effects on both humans and the

environment. Therefore, it is necessary to develop and investigate new methods to eliminate such pollutants from the aqueous environment.[11]

The removal of water contaminants become a major concern in the recent decade, and people are paying great attention to the problems related to environmental pollution that affect their health.

Most conventional wastewater treatment methods that have been developed to limit the pollution problem such as activated sludge, sand filtration, and coagulation-flocculation are inefficient in the removal of the chemical pollutants and eliminate the majority of the polluting compounds because they suffered from some limitations such as the lack of information about the potential effects of the compounds used on the environment, high solubility, bad removal efficiency, high cost,[7-14] and the possibility of desorption. So leads to the accumulation of the remaining quantities of pollutants in water.[1-6]

Consequently, the removal of Pharmaceutical compounds requires developing new efficient and effective treatment methods in order to face the problem of increasing water pollution and to provide improved sanitation and safe drinking water.[15]

1.2. Methods of pharmaceutical removal

Conventional wastewater treatment processes like activated sludge, sand filtration, and coagulation-flocculation are unable to eliminate recalcitrant pharmaceuticals from polluted water; however, the advanced treatment technologies are designed to achieve this. [16-17]

The aim of the coagulation-flocculation process is to aggregate the fine particles into larger particles to reduce suspended pollutants in wastewater. The coagulation process is done by adding a coagulant, followed by flocculation to increase the size of particles. This process leads to unstable pollutant particles causing sedimentation. These techniques involve pH adjustment and additions of some materials such as coagulants to increase the amount of precipitated materials. [18,19,20]

Recently, advanced treatment technologies such as advanced oxidation and adsorption by activated carbon have received much attention, however the results showed incomplete removal andexpensive cost.[21-22]

The oxidation technique was successfully applied to convert the organic pollutant residues in the wastewater. Remediation of trace organic pollutants with oxidizers has the ability to eliminate the organic contaminant, but oxidizing intermediates during the oxidation process are preventing complete elimination.

Mineralization of trace organic contaminants is the main target in choosing the type of technique used in the treatment process, to increase the possibility of reuse of treated wastewater in various applications. The Ozonation process is another technique used for pharmaceutical pollutants mineralization in wastewater, the advanced oxidation processes based on the hydroxyl radicals (•OH) as a primary oxidant. However, this method is not sufficiently effective in some cases because of the presence of some natural organic compounds such as bicarbonate, carbonate, and chloride ions in the wastewater. These compounds act as radical scavengers,

competing with pollutants for hydroxyl root consumption, as well as a relatively energy-intensive and high cost. Therefore, its presence increases the requirements for oxidation and reducestreatment efficiency. In addition, the pharmaceutical compounds are present in wastewater at very low concentration and this leads to an increase in the cost of processing treatment per unit mass.[23,24,25]

Membrane filtration is a separation technique, which has the ability to remove organic and inorganic pollutants as well as suspended solids. In these techniques, different types of membranes can be used for treatment of wastewater depending on the size of particles that will be attached to it.[26]

Three types of membrane filtration were commonly used, the first type of these membranes is ultrafiltration, in which a permeable membrane is used to separate

the suspended solid and macromolecules from wastewater. The second type is nanofiltration, where the membrane contains small pores and surface charge. These two properties give the membrane an advantage to reject charged solutes that are smaller than the membrane pores, and neutral solutes that are bigger than the pores. The third type of membrane filtration is reverse osmosis. The removal efficiency of these membranes depends on pressure difference across the membrane. Therefore, the higher the pressure, the higher the removal efficiency of pollutants in wastewater, which requires high energy.[27,28,29]

Membrane water treatment technology was found to be more effective in removing metals than organic contaminants such as pharmaceuticals. On the other hand, membrane fouling makes the operating cost of this method expensive.[30]

One of the alternative methods that has been used for the wastewater treatment is the adsorption technique. It is a surface phenomenon, which involves transferring substances from the liquid phase (adsorbent) to the solid surface (absorbent). Contaminants adhere to the solid surface through physical adhesion. However, a weak chemical bonding force sometimes occurs. It is a surface phenomenon, and it is the process of transferring the mass which a substance is transported from the liquid (adsorbate) phase to the surface of a solid (absorbent), and the contaminant compounds adhere at the surface of a solid by physical bonds, but sometimes weak

chemical bonding forces take place. The adsorption process is affected by different parameters such as the nature of adsorbate, type of adsorbent, temperature, presence of other pollutants, and the experimental conditions (contact time, the concentration of pollutant, the particles size of adsorbent, pH, and temperature). Due to its ability to remove biological, soluble and insoluble pollutants, adsorption technique has received extensive attention and wide range of applications.[27,31]

Activated carbon has good adsorption performance, due to its characteristics as an adsorbent including developed microspores, large surface area, and strong adsorption capacity, so it is widely used as a good adsorbent in water treatment. However, the widespread use of this technology has many limitations and is expensive. The filters used to separate contaminated activated carbon from the treated solution have a short service life, so these filters need to be replaced regularly, otherwise, the surface of these filters will be saturated and cannot be used for further purification.[32,33,34,35]

With the continuous spreading of the pharmaceutical residuals in the aquatic environment, the development of a cost-effective method and high capacity for removing the pharmaceutical contaminants from the aquatic environment has become an urgent necessity.[36]

Nanotechnology is applied to produce an effective nanomaterial for wastewater treatment. These nanomaterials have gained a lot of attention as eco-friendly and effective substances for removing pharmaceutical residues from wastewater. Because of their extraordinary properties such as high surface area, antimicrobial activity, magnetic properties, and photosensitivity, they have been used effectively for many applications. [37,38]

1.3. Diclofenac Sodium

Diclofenac sodium (DCF) is one of the 10 common drugs highly found in the aquatic environment [39] in superficial waters, wastewater, [40]and biosolids.[41] Because of its low biodegradability and higher consumption, about 940 tons/year produced in the world[4]. DCF is a non-steroidal anti-inflammatory drug (NSAID), analgesic, and antipyretic,[42] taken as oral tablets, suppositoriesor and injection.

DCF is a salt form of diclofenac, a phenyl ring with two chlorine atoms, and a benzene acetic acid derivative,[42] as in figure 1.1. It is considered a weak acid, insoluble in acidic solution (pKa=4.0), and soluble in water and intestinal fluid.[43]

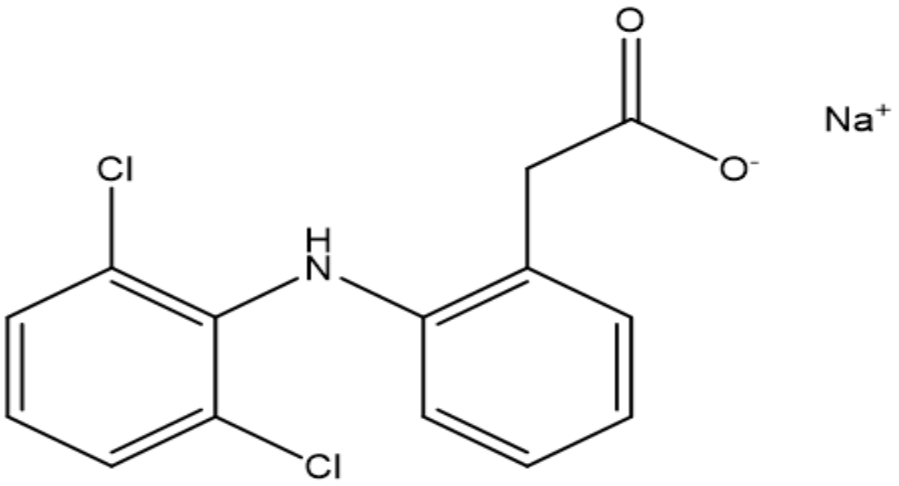

2-[(2,6-Dichlorophenyl)amino]benzeneacetic acid sodium salt

Figure 1. 1: Structure of DCF

The drug industry is the most source of DCF used for humans and animals. DCF is detected in the household and municipal wastewater treatment plants effluents, in addition to pharmaceutical industrial residue causing several risks for the environment and organisms.[44 -45]

The first and most widely case was a sudden collapse of vultures because they eating carcasses contain diclofenac, which causes nephrotoxicity.[44,46] Recent studies show that diclofenac could cause many diseases for mammals like hepatotoxicity, nephrotoxicity, cardiotoxicity, neurotoxicity, hepatotoxicity, and genotoxicity. However, if diclofenac concentration range from ng L^{-1} to µg L^{-1}, a diverse, toxic, and harmful effect on aquatic organisms will happen such as damage renal and

gastrointestinal tissue for many vertebrates like fishes, and affects the growth of its eggs.[44,46]

If 50 µg L^{-1} of diclofenac accumulates in the aquatic organisms, it causes terrible damage to the liver, kidney, and gill. For example, in rainbow trout, the accumulation of diclofenac in gill, liver, and muscle tissue leads to cytological changes even at 1 µg L^{-1}, else it causes lipid peroxidation and damage of tissue for mussels, and changes in the metabolism and the growth of blue mussels that are common in the Baltic Sea. Finally, diclofenac could accumulate in plants and can cause cytotoxicity and genotoxicity.[44,46]

The concentration of diclofenac differ according to water type:In surface water between (2002 -2019), the range was from <0.1 µg L^{-1} to 23.5 µg L^{-1} in most countries of the world, except for Nigeria and Portugal, it was above 35 µg L^{-1}. [46]

In groundwater, diclofenac exists because of leaching from landfills, surface water which contaminated with diclofenac, especially livestock farms that are the most source of contamination. The leaking from sewage and sewer pipes are minor sources of contamination. Globally the concentration of diclofenac in the groundwater is between (2.5 ng L^{-1} - 13.48 µg L^{-1}).[46]

In drinking water (mineral water and tap water), the concentration of diclofenac is in the range of ng L^{-1}, because of an inefficient treatment process to remove all

quantity of diclofenac from drinking water, this is happen in countries such as France, Japan, Spain, and Sweden.[46]

In seawater, the highest level of diclofenac detected in the Red Sea in Saudi Arabia was (10.2 μg L^{-1}), in the Mediterranean Sea (1.5 μg L^{-1}), and 241 ng L^{-1} in the Africa ocean, after that the levels become lower in other seas, oceans, and Gulfs.[46]

1.4. Removal of DCF from Water

Several methods are applied to remove DCF from water. The most widespread and effective one is adsorption, which removes organic and inorganic pollutants from water. It has more features than other methods like simplicity, high-quality, low energy consumption, effective cost, and a possibility for adsorbents to reuse and regenerate. The process converts the pollutant from liquid to the solid phase by two-dimensional interaction to the adsorbent surface, therefore reducing the bioavailability of these contaminants in the living organisms.[7,47,48] Several parameters can control the adsorption efficiency, such as adsorbent type, temperature, adsorbate properties, pH, and other experimental conditions.

Recent studies have shown several adsorbents like clay,[47] activated carbon,[7,48] graphene,[49] and expanded graphite were used as an adsorbent or as composite for DCF removal in an aqueous solution.[50] They have good efficiency for minimizing the percentage of DCF, but the number of adsorption recycles and reusing of these adsorbents is limited.

The presence of a negative charge on DCF inhibits the efficient removal using clay. Chemical modification for clay by intercalation of organic cations of the surfactant to produce an organoclay, which has a property for both hydrophobic environments and inorganic layered clay. Spectroger type C is an example of organoclays for the removal of organic pollutants from wastewater like DCF. Maia et al. found the removal efficiency of Spectroger was 99%, and adsorption capacity was 9.85 mg g $^{-1}$.[47]

The unique properties of activated carbon (AC) make it an excellent adsorbent for the treatment of industrial Wastewater. It has a high pore structure and a high specific surface area. Saucier et al, used Cocoa shell activated carbon for removal of the DCF, the removal efficiency was 97%, and the maximum adsorption capacity was 63.47 mg g $^{-1}$, while Sotelo et al. and Jung et al. used powdered activated carbon for DCF treatment, they found the maximum adsorption capacity equal 233.4 mg g^{-1} and 372 mg g $^{-1}$, respectively.[7]

Reis et al. Prepared AC from powdered sewage sludge and activate it with $ZnCl_2$ the results showed that the maximum absorption capacity of DCF was 156.7 mg g^{-1}. Also, Bhadra et al. investigate that oxidized activated carbons (OACs) which was a good adsorbent that enhanced the removal efficiency of DCF (~ 6 times) more than commercial AC.[48]

From the graphene family, Jauris et al. used a reduced graphene oxide rGO for the treatment of DCF, the study found that the maximum absorption capacity was equal to 59.67 mg g^{-1}. [49]

Expanded graphite or modified graphite has a specific surface area between 600 - 900 m^2 g^{-1}, which is very interesting for using as an adsorbent for pollutants in aqueous solutions. Vedenyapina et al. demonstrated that expanded graphite recovered 98 - 99% of DCF from aqueous solutions.[50]

1.5. Nano Zero Valent Iron (nZVI)

Solids nanoparticles have a high potential in applications of the adsorption process and are considered a useful method for the removal of pollutants from wastewater. Iron compounds of nanoparticle size are perhaps one of the first nanoscale technology products. It is efficient for the treatment of organic and inorganic contaminants and several heavy metals. Due to its large surface area, high reduction capacity, magnetic control, and simple recovery. Nano-zero valent iron nZVI (Fe^0)

is a type of iron nanoparticle that have an average diameter of 60 nm and have been used extensively in water treatment application, specifically for the separation and transformation of many contaminants due to the dual properties of Fe^0 nanoparticles, which consist of Fe^0 in the core and iron oxide shell. However, using nZVI for the treatment of wastewater suffers from some limitations. The two major weaknesses are the rapid oxidation of Fe^0 and lack of surface charge on Fe^0 which strongly leads the nanoparticles to agglomerate. Fe^0 particles tend to attract each other and aggregate to form a large size particle, resulting in a significant decrease in the surface area and activity of Fe^0. To solve this issue, researchers found various supporting materials to increase the stability and reduce particle aggregation for nZVI such as zeolite, bentonite, activated carbon, kaolinite, mesoporous silica, sepiolite, magnetite, hematite, goethite, and biochar.[51,52]

Carbon-based materials are highly significant in water treatments due to their properties: Stability in both acidic and basic media, large surface area, and a large number of active sites that are rich with functional groups.[53]

Activated carbon (AC) was used as a supporter for nZVI by synthesizing AC/nZVI composite. The composite enhanced the removal rate of Cr (VI) 2.2 times faster than AC.[54] Also, AC is used to progress the stability of nZVI for degradation and adsorption of chloramphenicol. It has been able to disperse the nZVI species and reduce the size of single particles.[55] Reduced graphite oxide impregnated by nZVI

was used for the adsorption of As (V) and As (III) from an aqueous solution and has been used as a supporter because of its high surface area.[56]

Besides, biochar is a solid-rich carbon; it has been got attention and is used widely as an adsorbent in water treatment investigation. Biochar is considered environmentally friendly and commercially available but is still limited in commercial applications due to the inability to recover.[57,58]

A composite of magnetic biochar synthesized as a potential adsorbent, the biochar made from peanut hull combines with Fe^0, was used for adsorption and degradation of Cr (VI) and trichloroethylene from solutions. Also, palladium and silicon-rich biochar-supported nZVI are used for the removal of Cr (VI). nZVI impregnated prepared for removal of copper ion from aqueous solution.[59]

Clay is a popular and commercially available adsorbent with low cost, non-toxicity, chemical stability, and high adsorption capacity because of the high specific surface area.[60] Kaolinite [61,62] , sepiolite [63], smectite [64], bentonite [65], and montmorillonite.[66] Zeolites [67] are clay materials that were used extensively in water treatment as adsorbents and supporters. A composite of clay supported nZVI is used in the remediation of contaminated aqueous solutions like dyes, heavy metals, selenite, nitrate, phenolic compounds, chlorinated organic compounds, and nitroaromatic compounds.[68]

1.6. Pencil Graphite

Pencil graphite (PG) gained considerable attention in scientific research due to its electrochemical and economic characteristics. Mostly, PG is composed of materials containing clay, graphite, and binder (wax) with different mixing ratios that determine the hardness and softness of PG. Pencils are marked with letters and numbers where the letter are H, B, and F. The letter H means a hard pencil (less graphite), the letter B indicates the blackness of a pencil (more graphite), and the letter F means a fine pencil, which has a sharpness much longer thane H and B, while the numbers indicate the degree of hardness.

Generally, pencils can be found with a mixture of these letters like HB (hard and black), HH (very hard), and BBB (deep black).[69] Pencil with HB type has a percentage mass of 0.68 of graphite, 0.26 of clay, and 0.05 of wax.[70] The ratio of clay to graphite has affected the morphology and properties of the PG.

PG gained much attention recently in electrochemistry due to its good electrochemical properties, affordability, availability, disposable ability, low electrical resistance (usually < 5 ohm), and surface ability for modification. It is used as an electrode, especially as a static standalone electrode for the detection of dopamine, ascorbic acid, morphine, and flavonoids. Further, it can use for the analysis of many organic and inorganic materials from very different matrices.[71,72,73]

The economic and electrochemical features besides the availability, and surface modification of PG, make them attractive for many applications in electro- analytical analysis, biological, and environmental fields instead of conventional electrodes based on noble metal.[71,74] However, many studies have presented that the hardness and roughness of pencil electrodes affected their performance and voltammetry response.[72]

1.7. The Purpose of this Study

Pencil graphite (PG) was used as a supporter material to increase the stability and dispersity of Fe^0 for the removal of DCF in an aqueous solution. In this study, a facial in-situ composite adsorbent from nZVI and pencil graphite (nZVI-PG) was synthesized, the composite was used to study the removal efficiency of DCF from an aqueous solution at different experimental conditions such as contact time, initial concentration of DCF, adsorbent dose, temperature, and pH.

The thermodynamic and kinetic parameters for the adsorption process of DCF via nZVI and (nZVI-PG) composite were studied by measuring the concentration of DCF in an aqueous solution before and after the adsorption using UV Spectrophotometry (UV-Vis). The synthesized nZVI nanoparticle and (nZVI-PG) composite were characterized using Transmission Electron Microscopy (TEM), X-

Ray powder diffraction (XRD), Energy-dispersive spectroscopy (EDS), and Fourier-transform infrared spectroscopy (FT-IR).

2. Experimental

2.1. Materials

All chemical reagents listed below were used without further purification:

Ferric chloride hexahydrate ($FeCl_3.6H_2O$, $\geq 99.5\%$) (Sigma-Aldrich Chemical Company) , Sodium borohydride ($NaBH_4$, $\geq 96\%$) (Merck),

Diclofenac sodium ($\geq$99%) (Merck), pencil lead graphite (HB) (Pilot),

Absolute ethanol (C_2H_5OH, $\geq 99\%$) (Merck), Milli-Q water,

Nitrogen gas N_2, hydrochloric acid (0.1M HCl),

Sodium hydroxide (0.1M NaOH), and sodium chloride (0.1M NaCl) (Sigma-Aldrich Chemical Company).

2.2. Calibration Curve of DCF Solutions

The initial concentration of diclofenac sodium (DCF) solution prepared was 100 mg/L, then a serial dilution was obtained to construct the calibration curve at the following concentrations 60, 40, 20, and 10 mg/L. The UV-visible Spectra for each

solution were measured using a UV-Vis spectrophotometer in the range of (200-400) nm at λ_{max} (276 nm).

2.3. Synthesis of nZVI and (nZVI-PG) Composite

2.3.1. Synthesis of nZVI

Nanoscale zero-valent iron (nZVI) was synthesized through the liquid reduction method as the following reaction: [51]

$$4Fe^{+3}_{(aq)} + 3BH^{-}_{4} + 9H_2O \rightarrow 4Fe^{0}_{(s)} + 3H_2BO_3^{-} + 12H^{+} + 6H_{2\,(g)}$$

4.84 g of ferric chloride hexahydrate was dissolved in a 100 ml solution of Milli-Q water and absolute ethanol with a volume ratio of 1: 4. The mixture was stirred by a magnetic stirrer until all of the ferric chloride hexahydrate particles dissolved, then 100 ml of reducing agent (0.47 M $NaBH_4$) was added slowly to the three-neck round bottom flask at a speed of 1-2 drops per second to reduce Fe^{+3} to Fe^{0} under continuous stirring and nitrogen atmosphere, the nanoparticles solution gradually changed to black color. When all $NaBH_4$ solution was added, the mixture should stay under stirring and nitrogen atmosphere for 20 minutes. Then, nZVI particles were collected by suction filtration under nitrogen gas and washed with absolute ethanol many times. Finally, nZVI particles were dried under a vacuum to prevent

the oxidation of nZVI particles.[75] Then the dried nanoparticles were stored in a glass bottle in the dark for future use.

2.3.2. Synthesis of (nZVI-PG) Composite

Facial and in-situ of the nZVI-PG composite were synthesized in a weight ratio of 1:1 of Fe^0 and PG. PG (HB-type) was milled by pestle and mortar, then the milled pencil graphite was added with ferric chloride hexahydrate in water/ethanol solution and the same procedures were followed.

2.4. DCF Removal Experiments

In this part, several parameters were investigated to study the removal efficiency of DCF via Fe^0 NPs and Fe^0-PG composite such as contact time, adsorbent dose, initial DCF concentration, pH, and temperature.

UV-vis spectrophotometer was used for measuring the absorbance of DCF, to determine the concentration of DCF in each step.

2.4.1. Effect of Adsorbent Dose

To determine the suitable mass of Fe^0 NPs that could be used to give a high removal efficiency for DCF, several experiments were performed by adding different masses of Fe^0: 20, 40, 80, and 100 mg in 100 ml of DCF solution with concentration of 20 mg/L, and was shaken at 110 rpm and 298 K. Then each solution was double filtrated using a syringe filter of 0.45µm, and a UV-Vis spectrophotometer was used to measure the absorbance of the solution at 276 nm to determine the concentration of DCF.

2.4.2. Effect of Contact Time and Adsorbate Concentration

The optimum concentration of DCF was determined by trying different initial DCF concentrations. In every trial, a fresh solution of DCF was prepared at an exact concentration.

A batch experiment was prepared for two types of NPs: nZVI and nZVI-PG composite. For nZVI an 80 mg of Fe^0 NPs was added to 100 ml solution of DCF at different concentrations: 20, 25, 30, 35, and 45mg/L. The solutions were shaken at 110 rpm for the contact time of 5, 10, 20, 30, 40, 60, 90, 120, and 150 min at 298 K.

For comparison study, 0.5 g of the nZVI-PG composite containing an effective mass of 80 mg Fe^0 was added to 100 ml of DCF solution at variable concentrations: 20, 25, 30, 35, and 45mg/L. The solutions were shaken at 110 rpm for a contact time of 10, 20, 30, 60, 90, 98, 120, 150, 190 min at 298 K.

Finally, a double filtration was done for each solution through a syringe filter of 0.45 µm, and the concentration of DCF was determined by measuring the absorbance at λ_{max} (276 nm) through a UV-Vis spectrophotometer.

2.4.3. DCF Removal Kinetics

The removal of DCF was studied as a function of time at an initial concentration of DCF equal to 20, 25, 30, 35, and 45mg/L and 80 mg of Fe^0 used in each of nZVI and nZVI-PG composite was added to 100 ml of DCF solutions and shaken at 110 rpm and 298K. Then the solutions were double filtrated through a syringe filter of 0.45µm. Finally, the absorbance of the solutions was measured using a UV-Vis spectrophotometer at 276 nm to determine the concentration of DCF.

2.4.4. Effect of pH and PZC

The effect of pH on DCF absorption by nZVI-PG composite was determined in a pH range from 4-9. The pH of 100 ml of 25 mg/L of DCF solutions was adjusted by 0.1M HCL and 0.1M NaOH to get the desired pH. After that, 0.5 g of the nZVI-PG composite was added to each solution and shaken at 110 rpm for 3 hours at 298 K. Then the removal effecincy and adsorption capacity are calculated.

The point of zero charge (PZC) for the nZVI-PG composite was investigated by adding 50 mL of 0.01M NaCl to a set of flasks and adjusting the pH for each solution by 0.1 M HCL and 0.1 M NaOH. The solutions pH was 2, 3, 4, 5, 6, 7, 8, 9, 10, and 11. Then 0.5 of the nZVI-PG composite was added to all the flasks and shaken at 110 rpm and 298 K for 24 hours. After that, the pH for each solution was recorded.

2.4.5. Effect of Temperature

The temperature effect was studied for the adsorption process. 80 mg of adsorbent was added to 100 ml of 25 mg/L DCF solution. The mixture was shaken in a thermostat shaker at 110 rpm at the following temperatures: 283, 288, 298, and 308 K. Final DCF concentration was determined after filtering by measuring the absorbance at a fixed wavelength of 276 nm using a UV-Vis spectrophotometer.

2.5. Characterization Techniques

Different techniques were performed for the characterization of the synthesized nZVI and nZVI-PG composite using UV-Vis, FT-IR, XRD, BET, SEM, and TEM. The presence of DCF on the surface of nZVI and nZVI-PG composite was investigated using FTIR and UV-Vis. The absorption spectra of the solutions were obtained by using an Agilent 8453 UV-Vis spectrophotometer that uses deuterium lamps and a photodiode array detector.

Fourier Transform Infrared Spectroscopy (FT-IR) spectra of DCF, nZVI and nZVI-PG composite and nZVI-PG with DCF were taken using (a Bruker TENSOR II Spectrometer). The spectra were measured using KBr pellets in the range of 4000-400 cm^{-1}.

The Powder X-Ray Diffraction (XRD) patterns of nZVI and nZVI-PG composite were collected by X-ray diffractometer instrument (Rigaku ultima) with a CuKα source and 2θ angle in the range 0 – 80° at a slow scan rate of 2θ min^{-1}.

By BET (Brunauer, Emmett and Teller) instrument (Autosorb iQ Quantachrome) the surface area for the PG before and after modification with nanoparticles was measured at relative pressures between 0.01 and 1.00. The liquid nitrogen adsorption-desorption isotherms were measured after degassing the material at 100-200°C to a pressure of 6.5×10^{-5} torr.

Scanning Electron Microscopy (SEM) was used to characterize the surface morphology, shape, and size of the nanoparticles using a scanning electron microscope coupled with energy dispersive X-ray (SEM-EDX) (Jeol 6700LV).

Transmission Electron Microscopy (TEM) images were obtained by JOEL-2100F field emission transmittance electron microscope (FE-TEM), with an accelerating voltage of 20 kV.

3. Results and Discussion

3.1 Characterization of nZVI and nZVI-PG Composite

nZVI and nZVI-PG composite were characterized by SEM, TEM, EDS, XRD, and FT-IR.

The surface morphology of nZVI and nZVI-PG composite was studied using SEM and TEM techniques. The morphology of nZVI is shown in Figure 3.1(a) and Figure 3.1 (b), which appear as a chain-like structure of spherical NPs with an average diameter of 60 nm. The magnetic interaction between NPs leads them to aggregate[76] and form the chain-like structure, this aggregate structure decreases the surface area of the NPs and limits their dispersion in the solution, therefore reducing the removal efficiency of the pollutants.[77] The shape of PG used in the synthesis of the nZVI-PG composite is shown in Figure 3.2(a) and Figure 3.2 (b). The images showed the milled PG as flakes and sheets.

The distribution of nZVI on the surface of PG is shown in Figure 3.3 (a). A heterogeneous composite was produced , and nZVI particles was well dispersed over the PG surface. This provide an indication that the aggregation between nZVI particles was reduced.

The NPs are tightly stuck and well dispersed on the surface of PG, and the Fe^0 NPs are not separated from PG using an external magnetic field, this characteristic makes the separation of composite to reuse is viable.

The SEM image in Figure 3.3 (b) shows the Fe^0-PG composite after adsorption of DCF on its surface, DCF layers approximately cover the surface of nZVI.

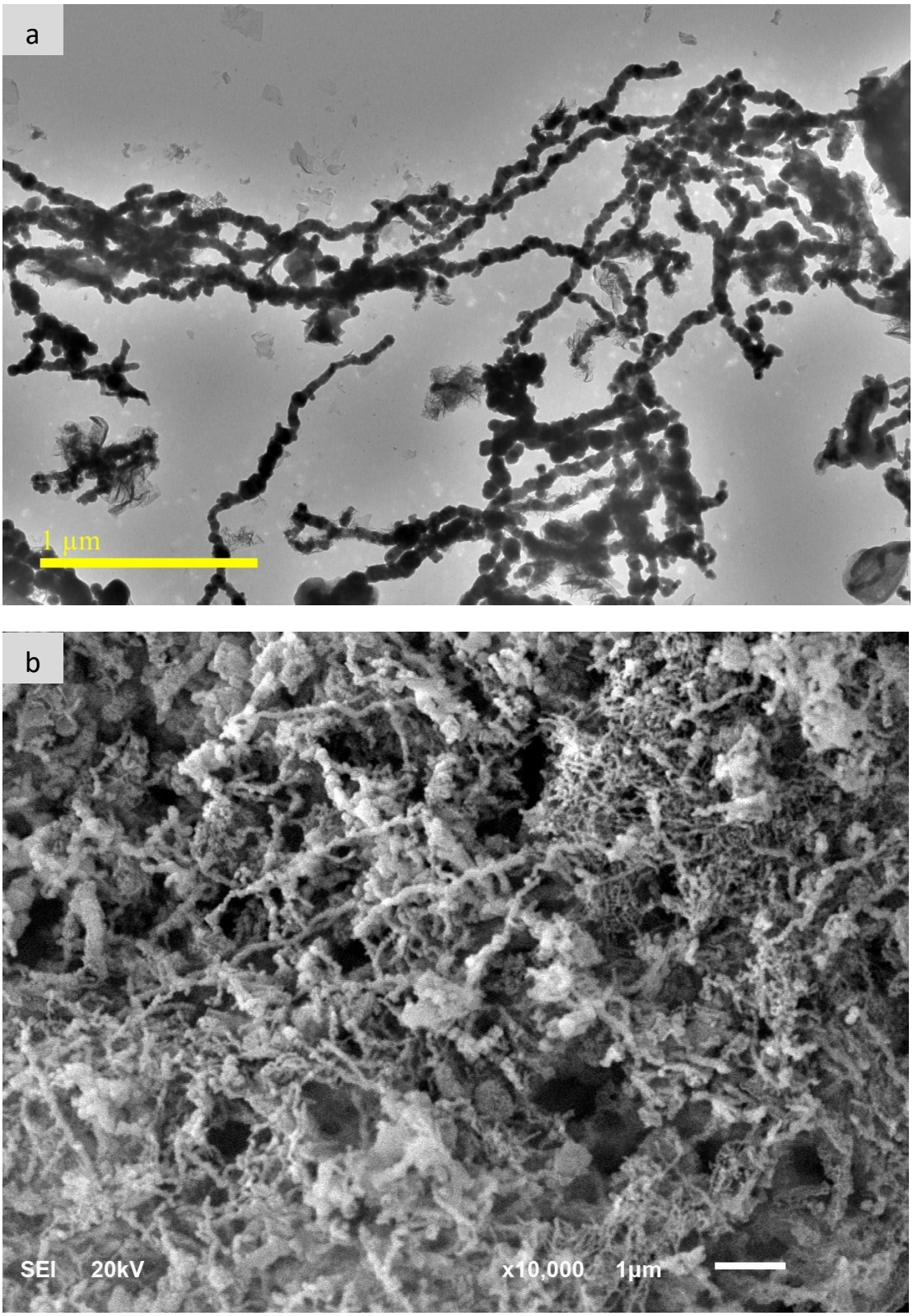

Figure 3. 1: (a) TEM, (b) SEM images of nZVI

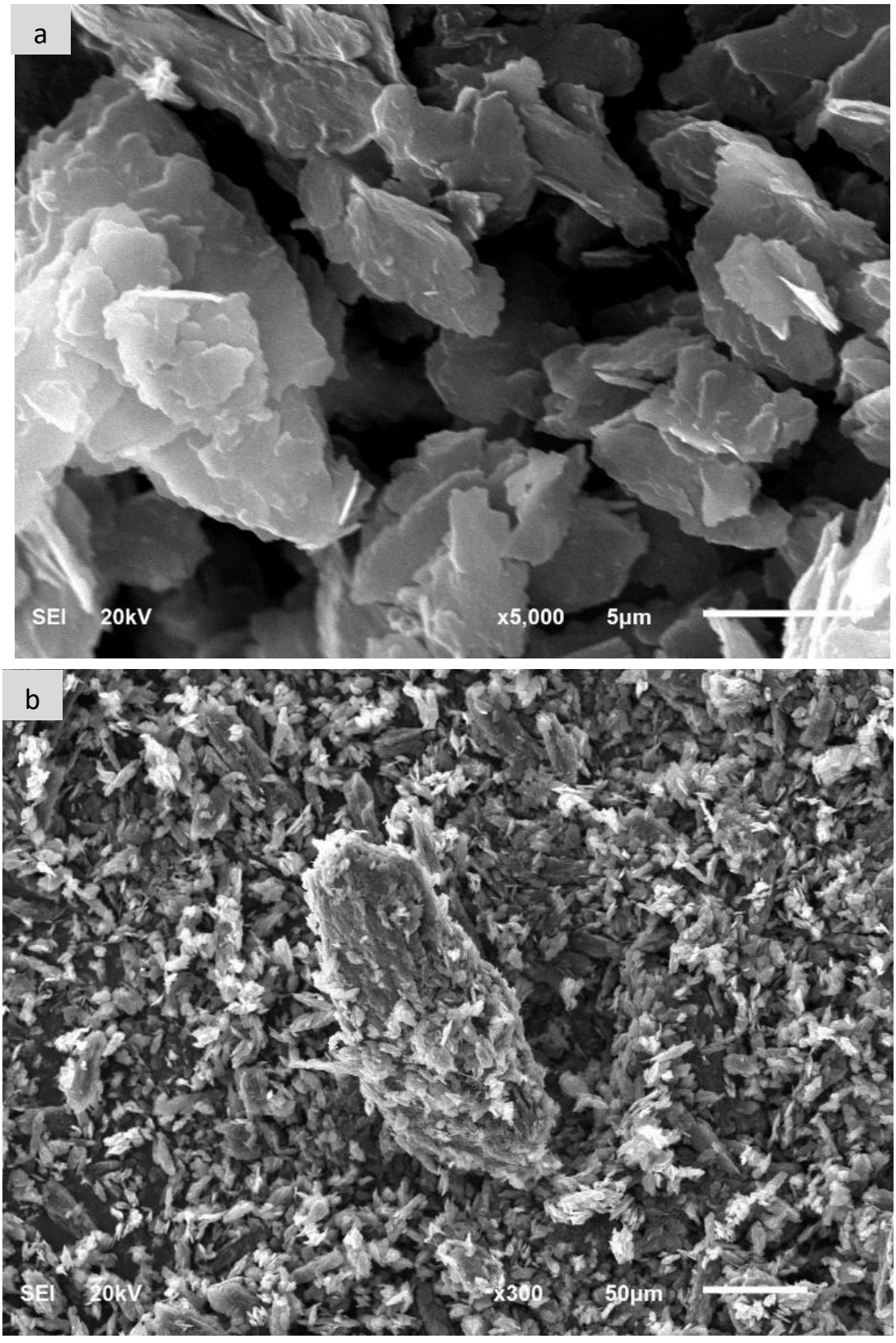

Figure 3. 2: (a) and (b) are SEM images of PG at different magnifications.

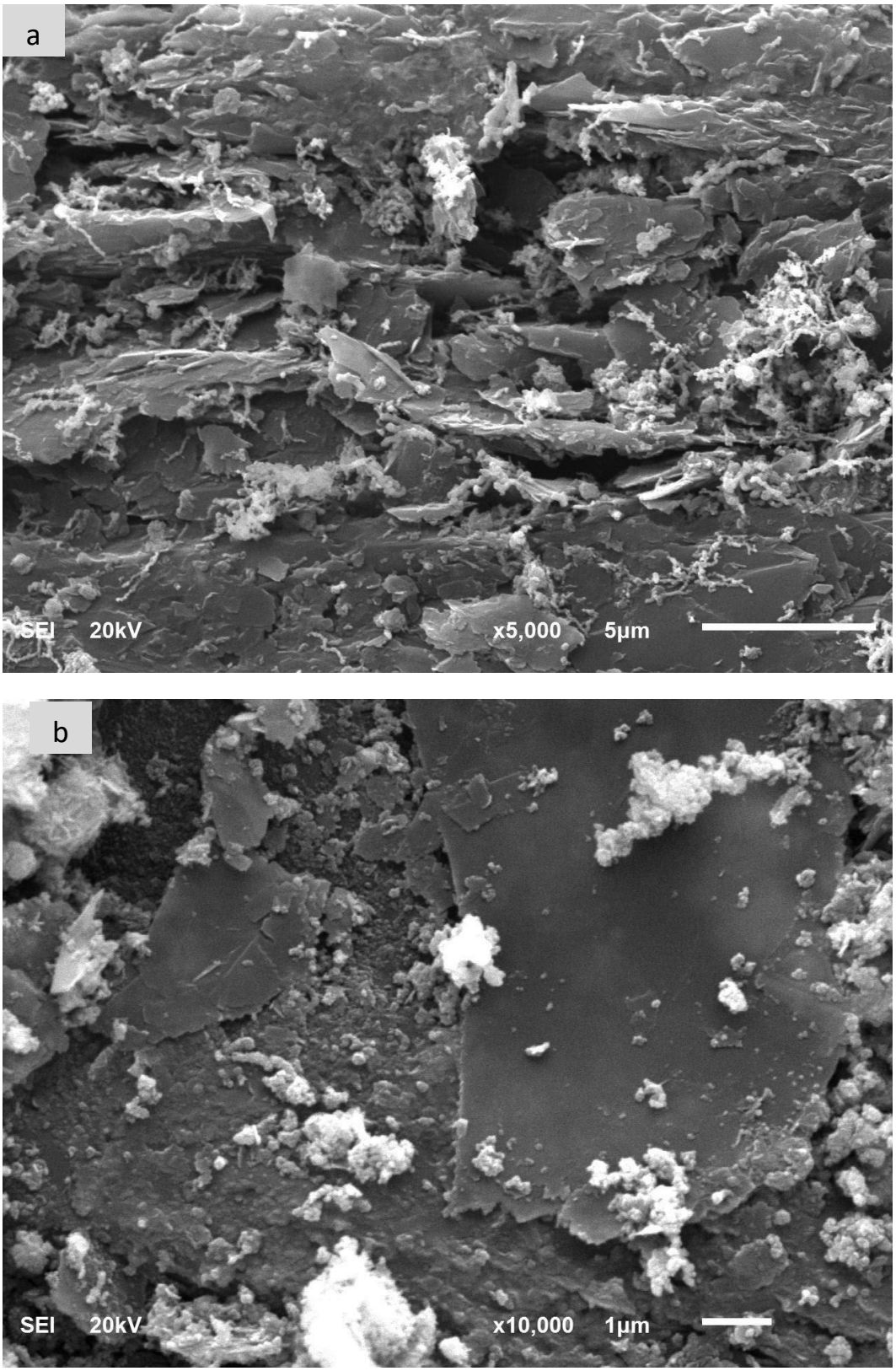

Figure 3. 3: (a) and (b) are SEM images of the nZVI-PG composite before and after DCF adsorption, respectively.

The elemental composition of the nZVI-PG composite was studied by the Energy-dispersive spectroscopy (EDS) using a Scanning electron microscope coupled with energy dispersive X-ray (SEM-EDX) (Jeol 6700LV). The analyzed area of the nZVI-PG composite is shown in Figure 3.4 (a). The EDS pattern indicates the presence of Fe, C, O, and Si elements as shown in figure 3.4 (b), which matches the expected results.

During EDS weight% analysis in Table 3.1, it is clear that the main constituent of adsorbent was Fe. Also, C has a high weight% because it is the main constituent of the supporter material (PG). Si and O elements are coming from clay that is used in the manufacture of PG,[78] while Au is used as a coating material to enhance the conductivity of the particles and the resolution of the instrument. Other details of the EDS spectra are shown in Table 3.1.

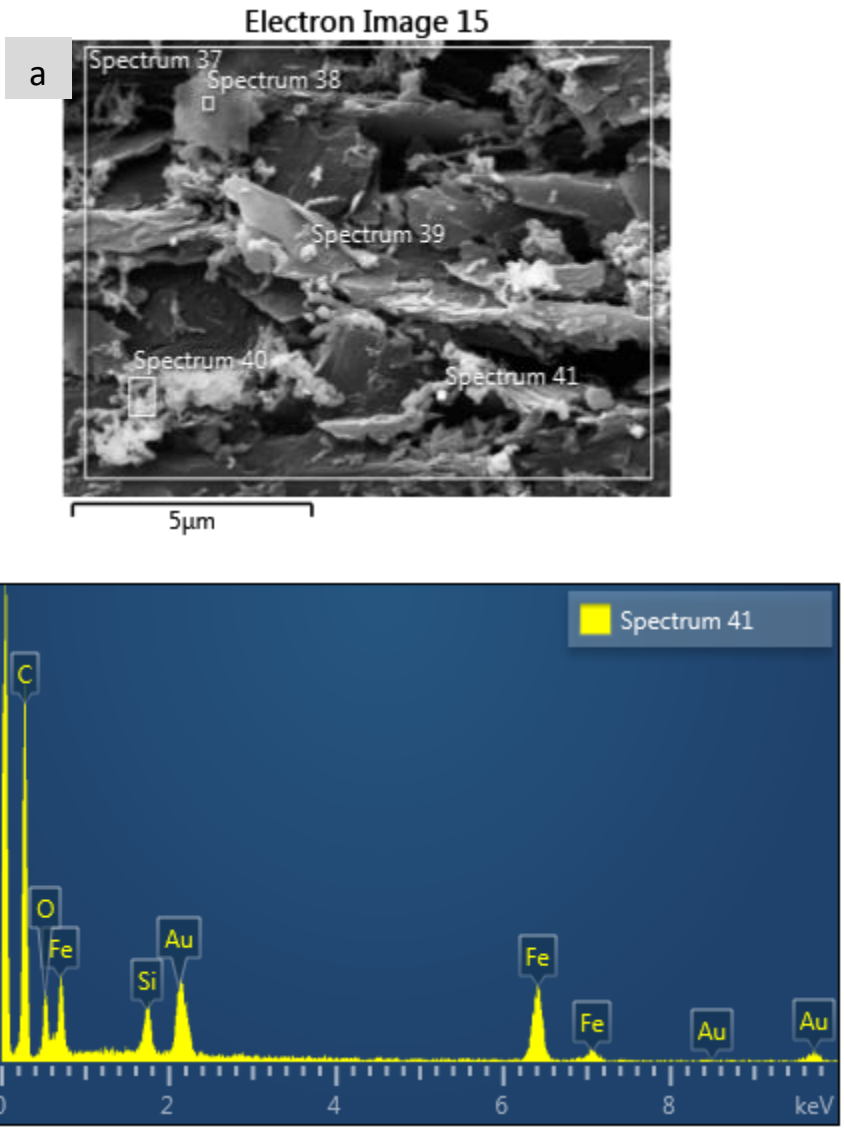

Figure 3. 4: EDS analysis of nZVI-PG composite

Table 3. 1: Elements analyzed of nZVI-PG composite.

Element	Line Type	Apparent Concentration	k Ratio	Wt%	Wt% Sigma	Standard Label	Factory Standard
C	K series	42.34	0.42335	68.86	1.14	C Vit	Yes
O	K series	11.46	0.03856	17.27	1.14	SiO_2	Yes
Si	K series	2.87	0.02273	1.50	0.13	SiO_2	Yes
Fe	K series	21.50	0.21498	12.37	0.51	Fe	Yes
Total:				100.00			

The XRD characterization techniques were used to determine the crystalline morphology of the nZVI and nZVI-PG composite, the diffraction pattern of nZVI and nZVI-PG composite is shown in Figure 3.4. The sharp peak at 2θ values of about 44.6° illustrates that distribution of small crystal particle size of metallic iron (Fe^0) with a crystallographic plane of (110) refers to (α-Fe) phase with a body-centered cubic crystal structure[76,79] Figure 3.5 (a). The XRD pattern of PG exhibited the (002) and (004) peaks at 2θ =26.2° and 54.0°, respectively, indicating that the pencil lead is made from natural graphite[80] Figure 3.5 (b). The XRD pattern of PG loaded with nZVI still showed a sharp diffraction of (002) and (004) peaks that assigned to PG has a crystal structure in the composite, while The last peak at 2θ = 44.6° with an index of (110) in the composite means the nZVI is attached to the PG surface[81] Figure 3.5 (c).

After adsorption of DCF by nZVI loaded on the PG surface, all peaks become broader and shifted to the right which indicates the attachment of DCF on the surface of Fe^0 NPs Figure 3.5 (d).

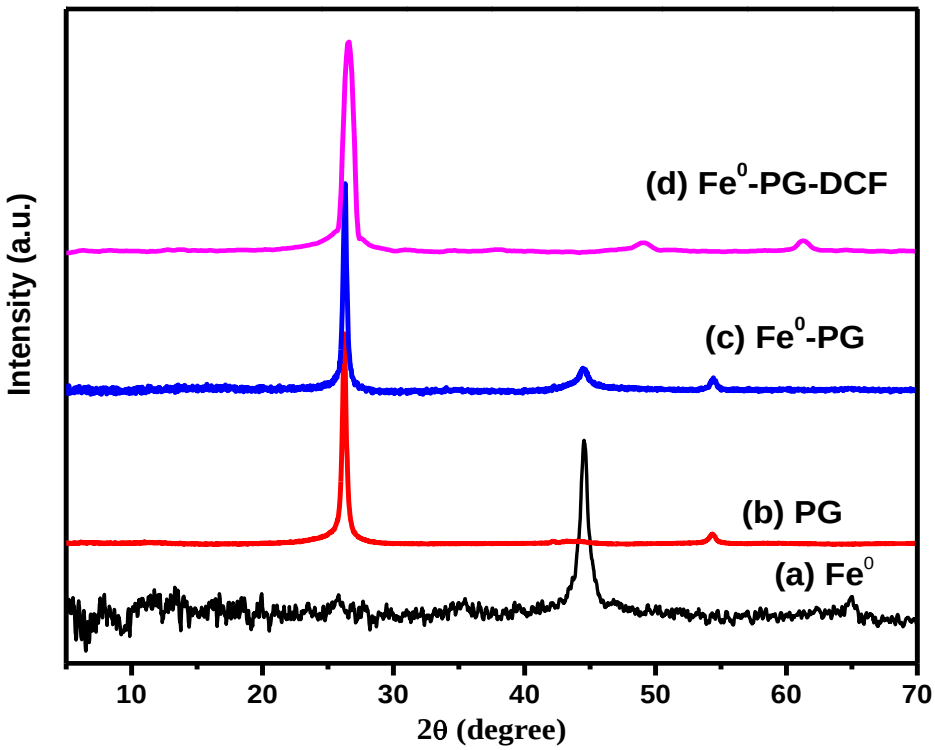

Figure 3. 5: XRD patterns of (a) Fe^0 NPs, (b) PG, (c) Fe^0-PG composite, and (d) Fe^0-PG-DCF.

FT-IR spectroscopy was used to identify the surface functional groups of the nanoparticles before and after the adsorption of a DCF. The FT-IR spectra of DCF and nZVI-PG composite before and after adsorption are presented in Figure 3.6. The FTIR spectra of DCF show an absorption band at 3386 cm^{-1} refers to N–H stretching, and absorption bands at 1192 cm^{-1} and 1168 cm^{-1} are attributed for C–N stretching in secondary amines. The strongest characteristic absorption bands intensities at 1574 cm^{-1} and 1452 cm^{-1} are due to COO^- asymmetric stretching and symmetric stretching, respectively. The absorption band at 1504 cm^{-1} is assigned for C=C

stretching vibrations in an aromatic ring, while the adsorption band of C-Cl stretching vibrations is presented at 766 cm^{-1} and 745 cm^{-1} [82] Figure 3.6 (a).

The FT-IR spectrum of Fe^0- PG composite Figure 3.6 (b) shows characteristics bands at 3428 cm^{-1} for O-H stretching vibration which may be originated from the FeOOH group on a surface of and nZVI or from water absorbed by nZVI. And at 1633 cm^{-1} and 803 cm^{-1} that assigned for O-H bending which could be from the iron oxide shell.[83]

Finally, the adsorption bands at 1092 cm^{-1} and 1028 cm^{-1} indicate the presence of some γ-FeOOH lepidocrocite on the shell of Fe^0 NPs.

The FT-IR spectrum for Fe^0-PG-DCF Figure 3.6 (c) shows a formation of a new stretching vibration Fe–O band at 579 cm^{-1} .[83] After adsorption of DCF all bands were shifted to the right because of the increase in the molecular mass of the vibrating molecules that is inversely proportional to the frequency.

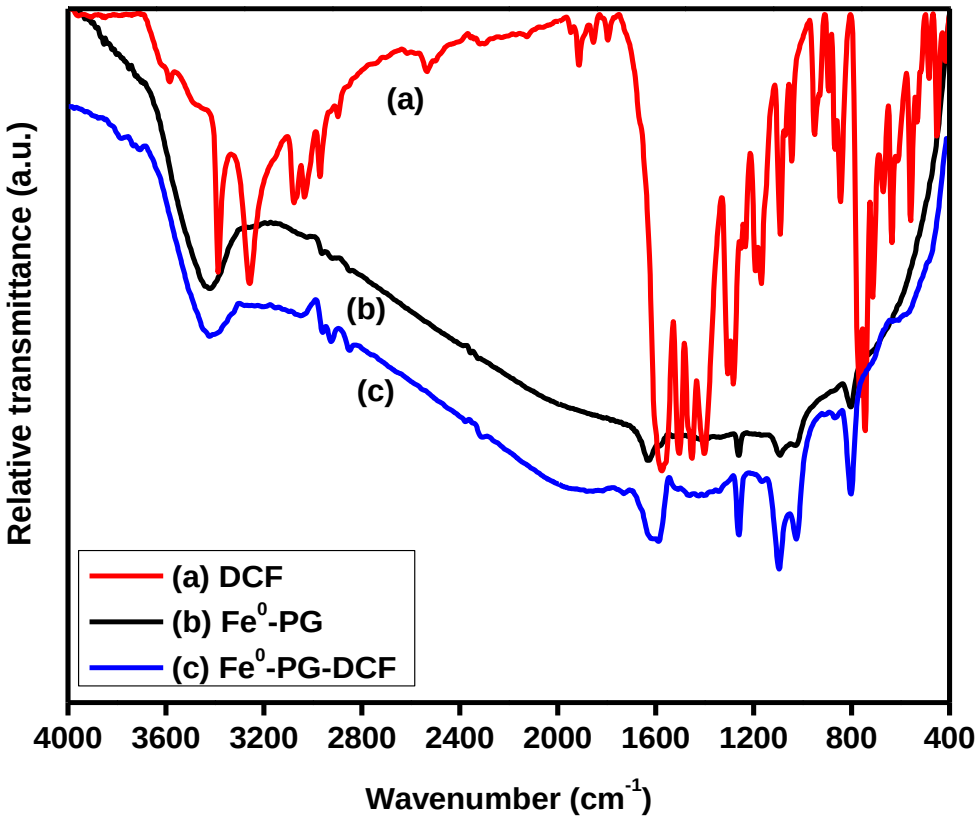

Figure 3. 6: FT-IR spectra for: (a) DCF, (b) Fe^0-PG composite, and (c) Fe^0-PG-DCF.

In addition, the surface area was measured using the BET technique, the data presented in Table 3.2, the results show that the surface area of Fe^0 is larger than both PG and Fe^0-PG, while the Fe^0-PG composite has a larger surface area than PG.

Table 3. 2: The surface area for Fe^0 NPs, PG, and Fe^0-PG composite.

Type	Surface Area (m^2/g)
Fe^0 NPs	131.2675
PG	2.7237
Fe^0-PG composite	88.56

3.2. Effect of Fe^0 NPs Dose

The effect of Fe^0 NPs dose on the removal efficiency of DCF was studied at different masses of Fe^0: 20, 40, 80, and 100 mg at 298K. The percentage removal equation (2) was used to calculate the percentage removal of DCF as shown in Figure 3.7.

The results show that the higher % removal of DCF was at 80 mg of Fe^0 which has high active sites on the surface of NPs. This mass is considered an effective mass and will be taken as a standard for the later experiments and calculations.

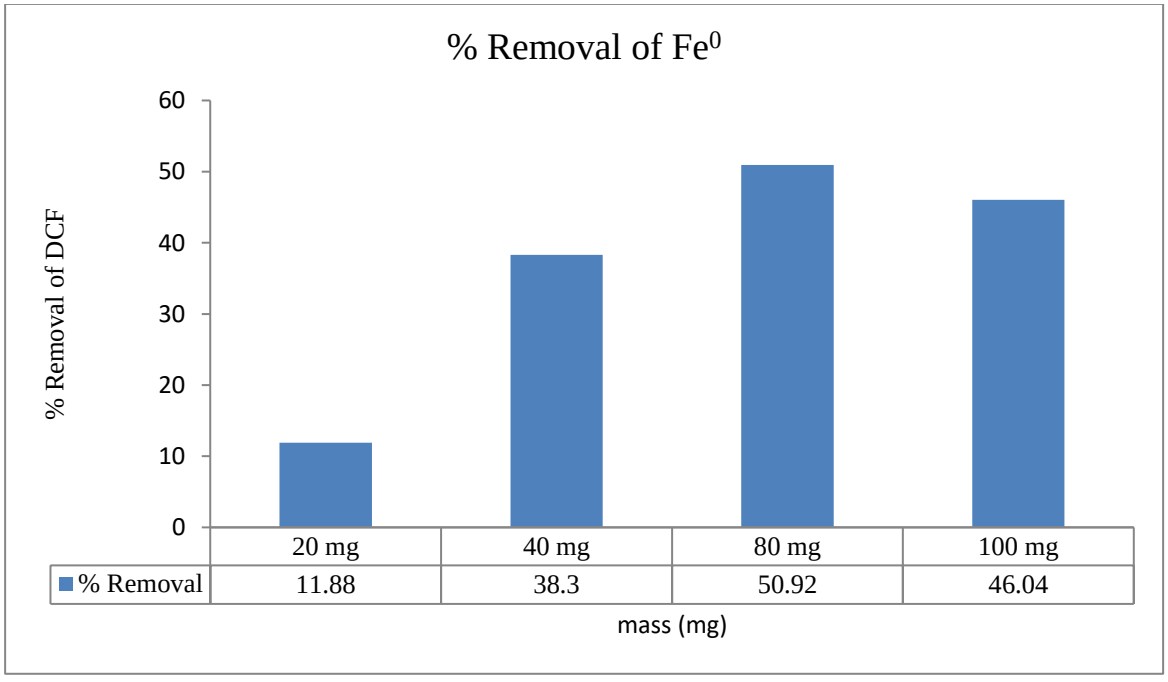

Figure 3. 7: Effect of Fe^0 NPs dose on the % removal of DCF.

3.3. Adsorption Kinetics

The kinetic adsorption of DCF and rate of adsorption process were studied in this part depending on kinetics experiments performed. The adsorption of DCF onto the surface of Fe^0 NPs and Fe^0-PG composite were investigated at different concentrations of DCF: 20, 25, 30, 35, and 45 mg/L as a function of time at 298 K. The amount of DCF adsorbed on the surface of Fe^0 NPs and Fe^0-PG composite was calculated using a mass balance equation: [84]

$$Q_t = (C_0 - C_t)\frac{V}{m} \qquad (1)$$

Where Q_t is the concentration of DCF on the adsorbent (mg/g) at a function of time,

C_0 is the initial concentration of DCF (mg/L),

C_t is the DCF concentration in the solution given at the time,

V is the volume of solution (L),

m is the mass of adsorbent (mg).

The effects of contact time on the DCF concentration adsorbed via two types of adsorbents are shown in Figure 3.8.

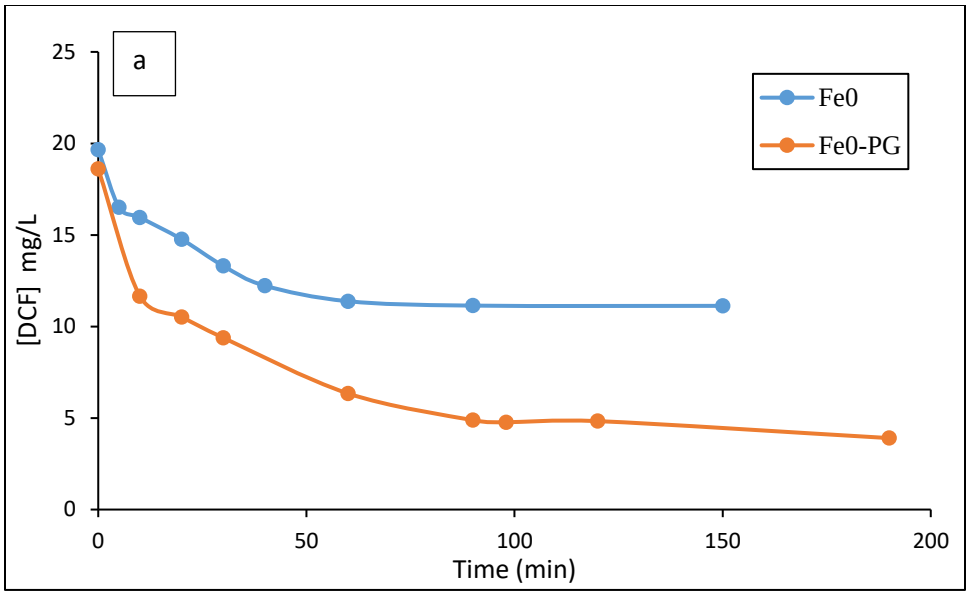
a
Fe0
Fe0-PG
[DCF] mg/L
Time (min)
0
5
10
15
20
25
0
50
100
150
200

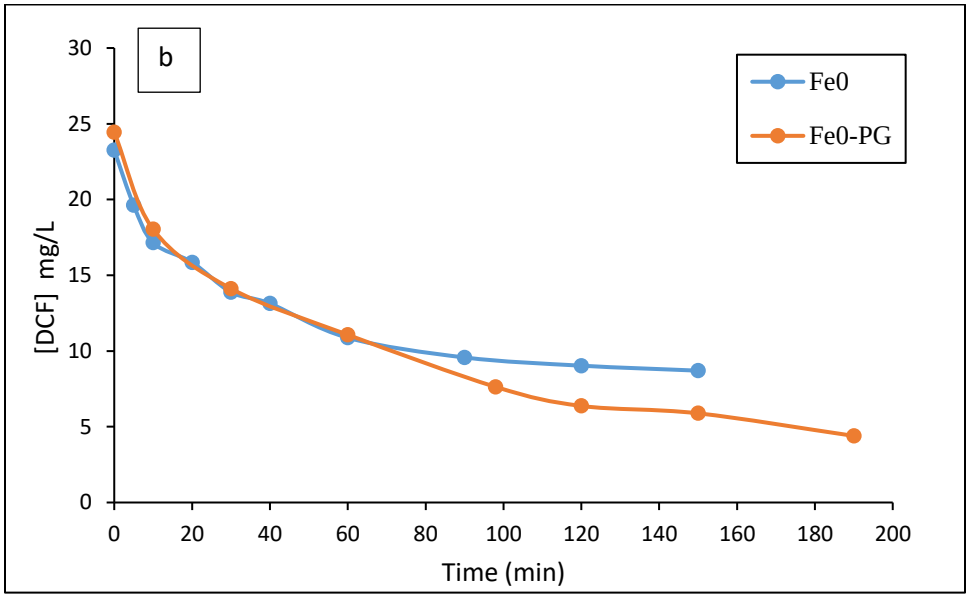
b
Fe0
Fe0-PG
[DCF] mg/L
Time (min)
0
5
10
15
20
25
30
0
20
40
60
80
100
120
140
160
180
200

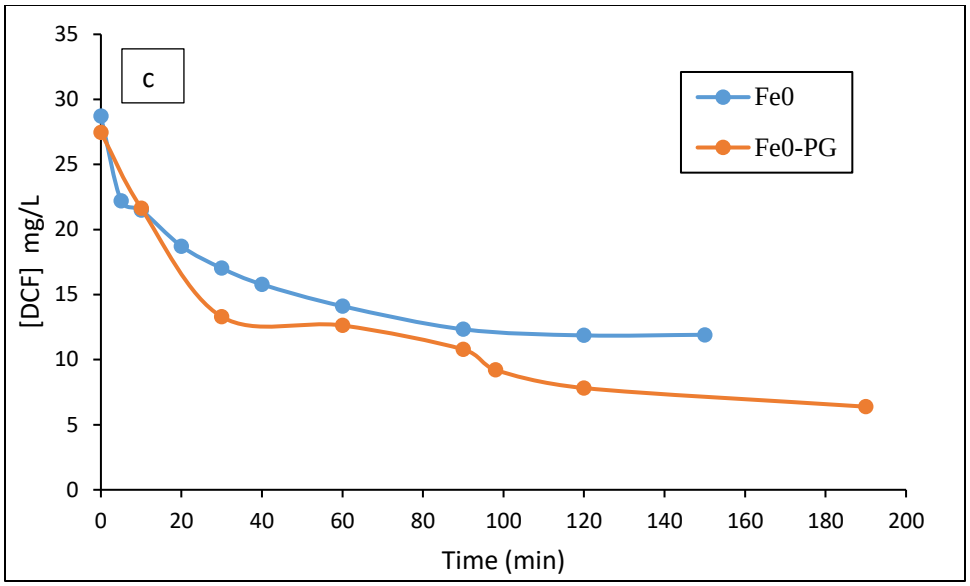
c
Fe0
Fe0-PG
[DCF] mg/L
Time (min)
0
5
10
15
20
25
30
35
0
20
40
60
80
100
120
140
160
180
200

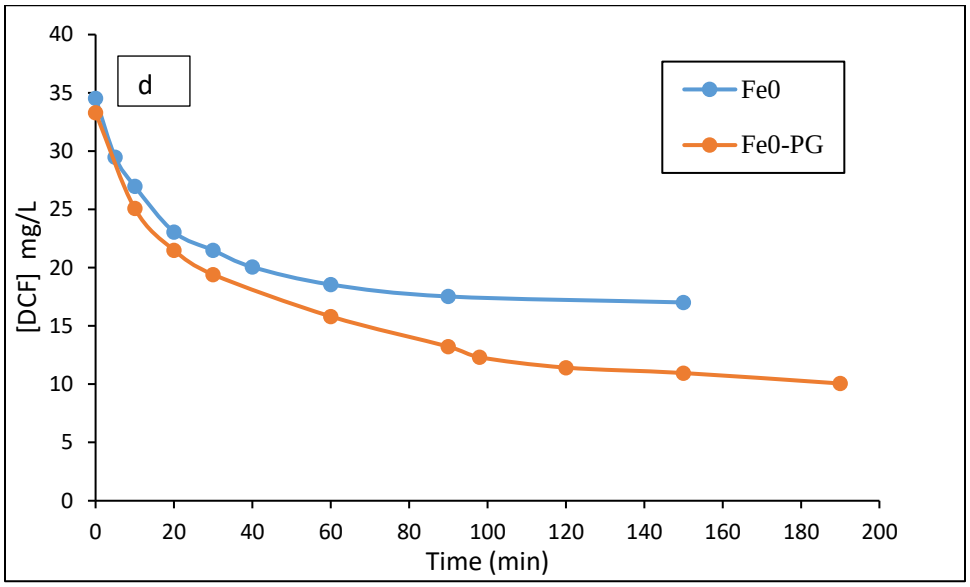
d
Fe0
Fe0-PG
[DCF] mg/L
Time (min)
0
5
10
15
20
25
30
35
40
0
20
40
60
80
100
120
140
160
180
200

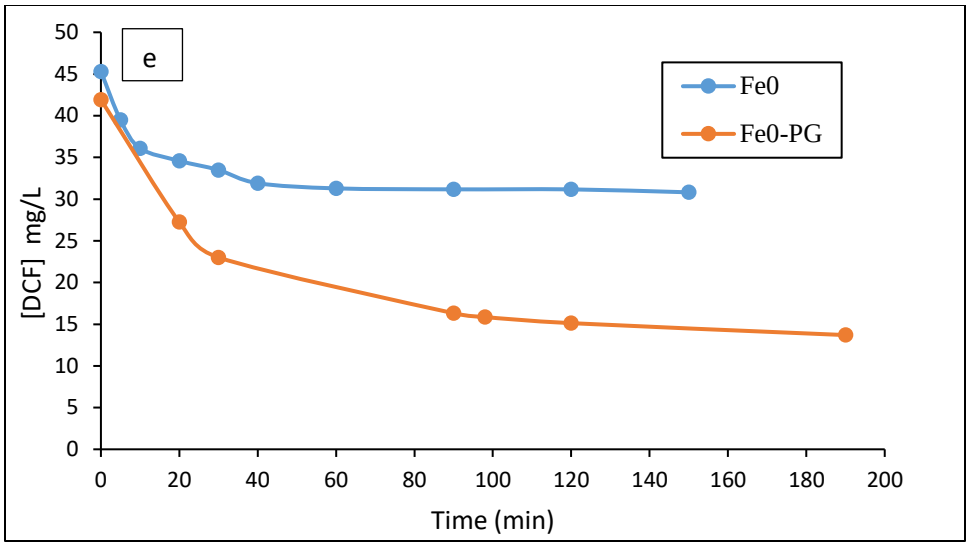

Figure 3. 8: Effect of contact time on the removal of DCF via Fe^0 NPs and Fe^0-PG composite; (a) 20 mg/L (b) 25 mg/L, (c) 30 mg/L, (d) 35 mg/L, (e) 45mg/L at 298K.

The figures show that Fe^0 NPs reach the equilibrium faster than Fe^0-PG composite, so the stop time of adsorption process for Fe^0 NPs was at 150 min while for Fe^0-PG composite was at 190 min.

.

The DCF removal percentage was calculated using the following equation: [85]

$$\%\ Removal = \frac{C_0 - C_e}{C_o} * 100\% \qquad (2)$$

Where C_0 is the initial concentration of DCF in the solution (mg/L),

C_e is the equilibrium concentration of DCF in the solution (mg/L).

The effects of contact time on the removal efficiency of DCF for the two types of NPs at different concentrations are shown in Figure 3.9.

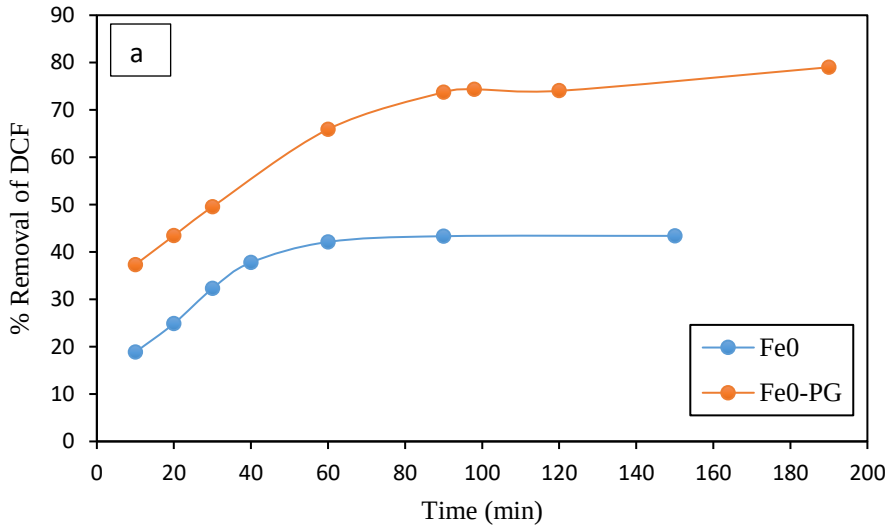

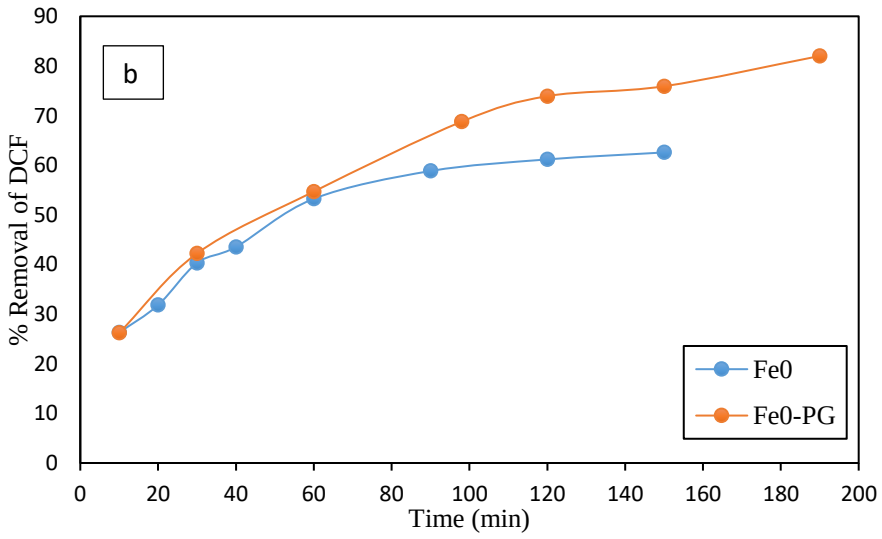

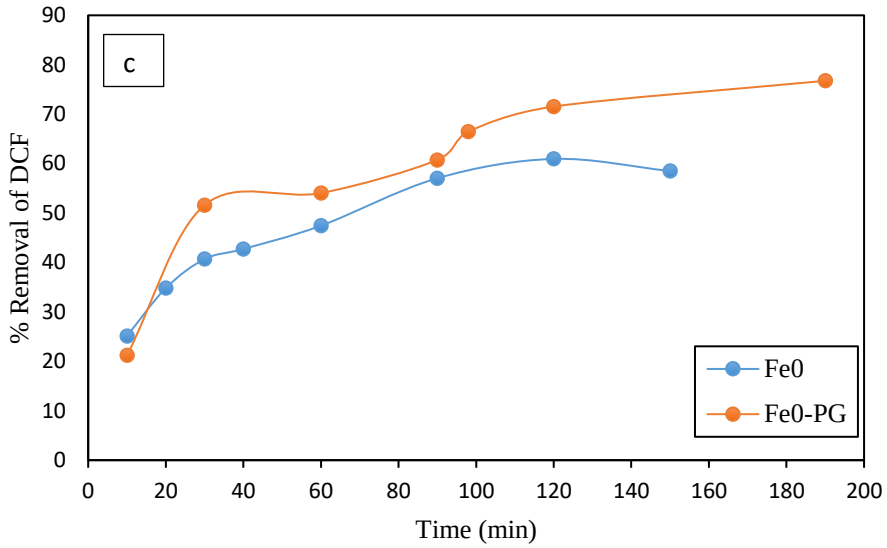
c
% Removal of DCF
Time (min)
Fe0
Fe0-PG
0
10
20
30
40
50
60
70
80
90
0
20
40
60
80
100
120
140
160
180
200

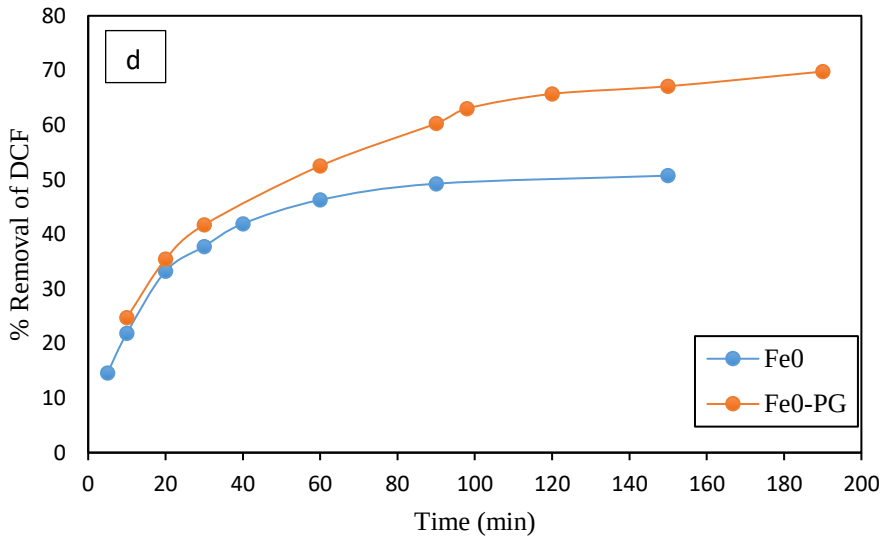
d
% Removal of DCF
Time (min)
Fe0
Fe0-PG
0
10
20
30
40
50
60
70
80
0
20
40
60
80
100
120
140
160
180
200

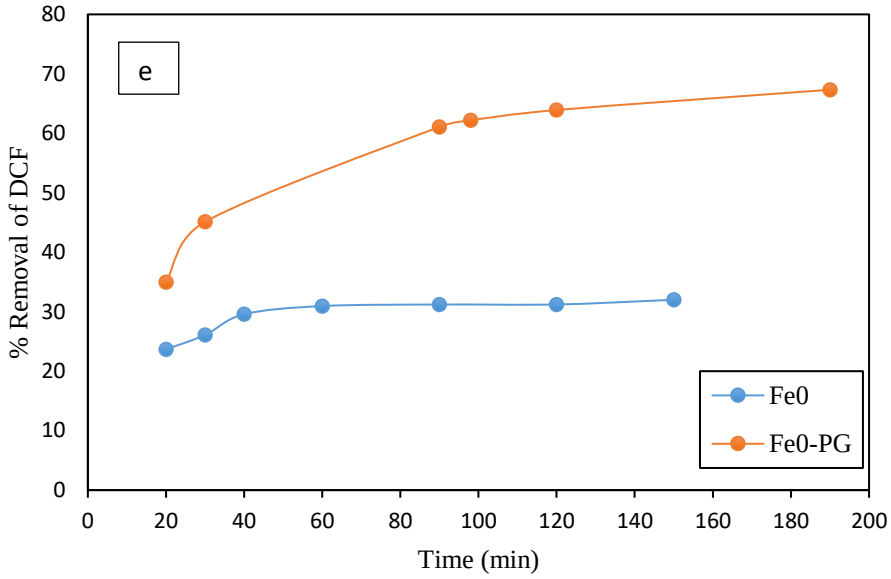

Figure 3. 9: Effect of contact time on removal efficiency of DCF using Fe^0 NPs and Fe^0-PG composite; (a) 20 mg/L, (b) 25 mg/L, (c) 30 mg/L, (d) 35 mg/L, (e) 45mg/L at 298K.

From Figure 3.8 and Figure 3.9, it's clear that the removal efficiency of DCF via two types of adsorbents increased with time since the concentration of DCF in an aqueous solution is decreasing with time. However, the concentration was decreased till the lowest after that almost approach the equilibrium.

The experimental data shown in Figure 3.8 for the adsorption of DCF onto Fe^0 NPs and Fe^0-PG composite were tested by Lagergren pseudo-first-order and pseudo-second-order models.[86] The nonlinear Lagergren pseudo-first-order model is represented as:

$$Q_t = Q_e(1 - e^{-k_1 t}) \qquad (3)$$

The linear Lagergren pseudo-first-order model represented as:

$$ln(Q_e - Q) = lnQ_e - k_1 t \qquad (4)$$

Where Q_e is the amounts of DCF (mg/g) adsorbed by the adsorbent at equilibrium, Q is the amounts of DCF (mg/g) adsorbed by the adsorbent at any time, k_1 is the first-order rate constant (min^{-1}), and t is the time (min).

A linear relationship is obtained by plotting ln(Qe-Q) versus time. The resulting figures of this relationship are plotted and attached in the appendix. The correlation coefficient (R^2) values obtained for Fe^0 NPs and Fe^0-PG composite are listed in Table 3.3, where the values of k_1 and Q_e are calculated from the slope and intercept, respectively.

Table 3. 3**:** The correlation coefficient (R^2) values from the linear fit pseudo-first-order for the adsorption of DCF via Fe^0 NPs and Fe^0-PG composite at 298 K.

C_0 (mg/L)	**R^2**	
	Fe^0 NPs	Fe^0-PG composite
20	0.7742	0.9083
25	0.9488	0.985
30	0.9255	0.93
35	0.8587	0.9582
45	0.8018	0.9219

Table 3.3 shows that the correlation coefficient (R^2) for the linear pseudo-first-order has low values and the data is not fitted with the pseudo-first-order model. So another kinetic model was examined to fit with the experimental data.

Also, the linear fits obtained by pseudo-second-order kinetics are shown in Figure 3.10.

The nonlinear pseudo-second-order form of the Ho equation is given as:

$$Q = \frac{k.t.Q_e^2}{1 + k.Q_e.t} \qquad (5)$$

The linearized pseudo-second-order model as given by Ho: [87]

$$\frac{t}{Q} = \frac{1}{k_2\, Q_e^2} + \frac{1}{Q_e}t \qquad (6)$$

Where Q is the amount of the DCF adsorbed on the adsorbent (mg/g),

Q_e is the amount of the DCF adsorbed on the adsorbent at equilibrium (mg/g),

k_2 is the rate constant of the pseudo-second-order adsorption (g mg^{-1} min^{-1}), t is the time(min).

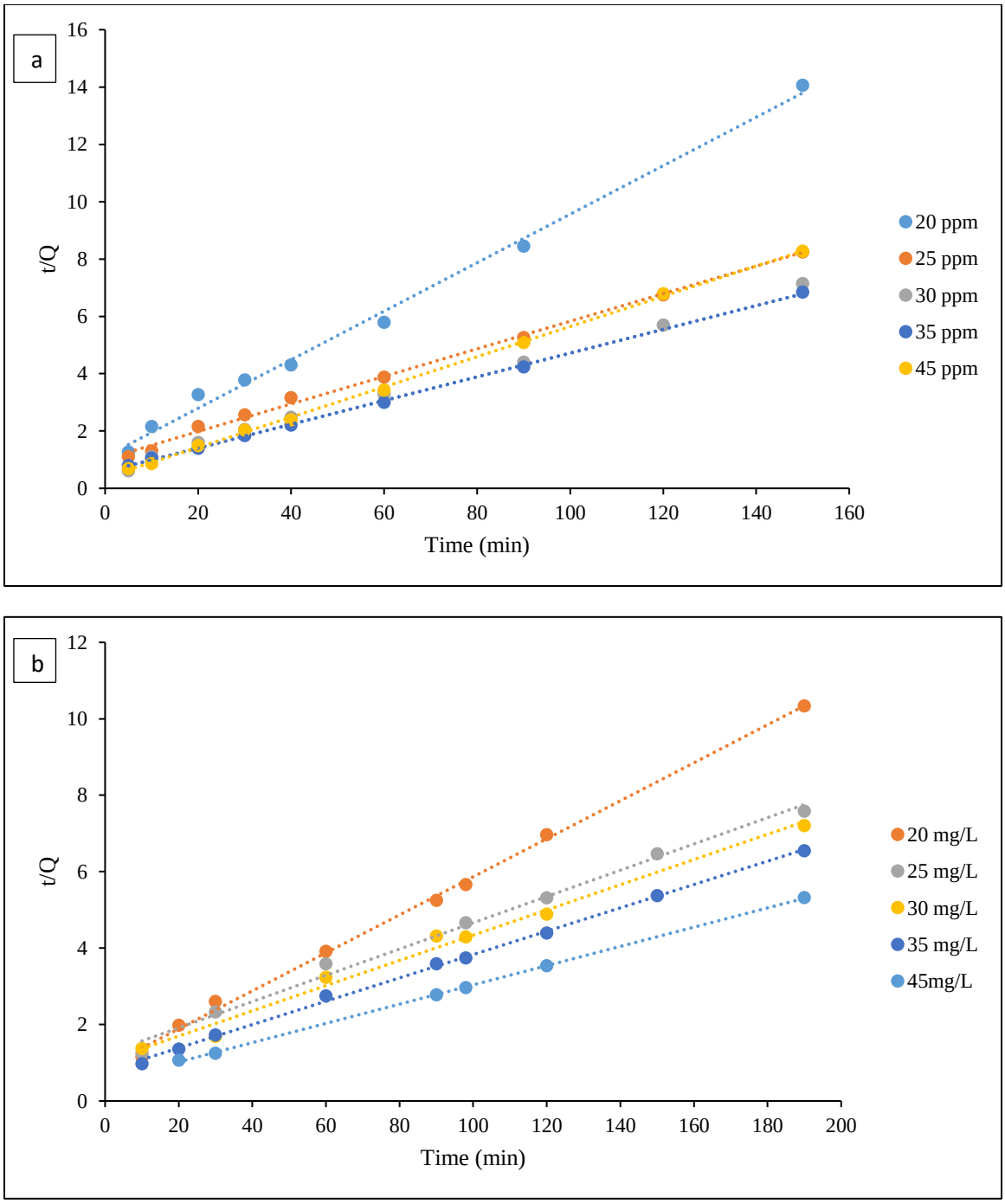

Figure 3. 10: The pseudo-second-order linear fits for DCF adsorption via a) Fe^0 NPs and b) Fe^0-PG composite at 298 K.

The kinetic parameters for pseudo-first-order and pseudo-second-order models for Fe^0 NPs and Fe^0-PG composite are demonstrated in Table 3.4 and Table 3.5. The data seems suitable well to the pseudo-second-order kinetics because most of the values of R^2 are larger than 0.99. In addition, in pseudo-second-order kinetics, the difference between the calculated values of adsorption capacity ($Q_{e,(cal)}$) and the experimental value of adsorption capacity ($Q_{e,(exp)}$) are less than the difference that exists in the pseudo-first-order model.

This means that the adsorption of DCF using Fe^0 NPs and Fe^0-PG composite are well represented by the pseudo-second-order model that was found it described well the adsorption of heavy metals.[88]

Table 3. 4**:** Kinetic parameters for DCF adsorption by Fe^0 NPs at 298K.

Pseudo-first order kinetics					Pseudo-second order kinetics			
C_0 (mg/L)	$Q_{e,exp}$ (mg g^{-1})	$Q_{e,cal}$ (mg g^{-1})	k_1 (min^{-1})	R^2	$Q_{e,exp}$ (mg g^{-1})	$Q_{e,cal}$ (mg g^{-1})	k_2 (g mg^{-1} min^{-1})	R^2
20	10.67	6.178	0.0146	0.7742	10.67	11.82	0.006492	0.9944
25	18.19	14.16	0.0128	0.9488	18.19	20.79	0.002268	0.9967
30	21.05	14.19	0.0131	0.9255	21.05	23.36	0.002797	0.9967
35	21.90	13.45	0.0138	0.8587	21.90	24.15	0.002969	0.9994
45	18.12	7.219	0.015	0.8018	18.12	18.98	0.007424	0.9993

Table 3. 5**:** Kinetic parameters for DCF adsorption by Fe^0-PG composite at 298K.

Pseudo-first order kinetics					Pseudo-second order kinetics			
C_0 (mg/L)	$Q_{e,exp}$ (mg g^{-1})	$Q_{e,cal}$ (mg g^{-1})	k_1 (min^{-1})	R^2	$Q_{e,exp}$ (mg g^{-1})	$Q_{e,cal}$ (mg g^{-1})	k_2 (g mg^{-1} min^{-1})	R^2
20	18.38	10.78	0.011	0.9083	18.38	20.12	0.002775	0.9976
25	25.05	21.36	0.0091	0.985	25.05	29.07	0.0009653	0.992
30	26.36	20.14	0.0092	0.93	26.36	30.30	0.001049	0.9885
35	29.03	20.93	0.01	0.9582	29.03	32.79	0.001198	0.9985
45	35.71	20.51	0.0097	0.9219	35.71	39.68	0.001225	0.9997

Furthermore, other models can be used to study the relation between the highest adsorption capacity (Q) and t. The pseudo-second-order rate equation is represented by the Shahwan equation, as shown in Figure 3.11. This model differs from the Ho model in the way of calculation of the rate constant and its unit, and the interpretation of Q_m.[89]

The nonlinear form of the Shahwan equation is given as:

$$Q = \frac{Q_m C_0 k_2 t}{C_0 k_2 t + 1} \qquad (7)$$

The linearized equation of this model is given in the following form:

$$\frac{t}{Q} = \frac{1}{Q_m C_0 k_2} + \frac{1}{Q_m} t \qquad (8)$$

Where Q is the amount of DCF adsorbed on the adsorbent (mg/g),

Q_m is the amount of DCF that would be sorbed if the sorption reaction approaches completion (equals to V/ m multiplied by C_0),

C_0 is the initial concentration of the DCF (mg/L),

k_2 is the rate constant (L mg^{-1} min^{-1}),

t is the time (min).

Table 3.6 and Table 3.7 shows the calculated kinetic rate constants of pseudo-second-order obtained from calculated Q values using equations (6 and 8), for Fe^0 NPs and Fe^0-PG composite.

Table 3. 6**:** The kinetic parameters for adsorption DCF using Fe^0 NPs of the pseudo-second-order linear fits using equations 6 and 8 at different concentrations at 298K.

Ho Equation	**20 mg/L**	**25 mg/L**	**30 mg/L**	**35mg/L**	**45 mg/L**
Slope	0.0846	0.0481	0.0428	0.0414	0.0527
R^2	0.9944	0.9967	0.9967	0.9994	0.9993
Intercept	1.1024	1.0202	0.655	0.5772	0.3741
k_2 ($g.mg^{-1}.min^{-1}$)	0.006492	0.002268	0.002797	0.001198	0.007424
$Q_{e\ (cal)}$ (mg/g)	11.82	20.79	23.36	24.15	18.98
$Q_{e\ (exp)}$ (mg/g)	10.67	18.19	21.05	21.90	18.12
Shahwan Equation					
Slope	0.0846	0.0481	0.0428	0.0414	0.0527
R^2	0.9944	0.9967	0.9967	0.9994	0.9993
Intercept	1.1024	1.0202	0.655	0.5772	0.3741
k_2 ($L.mg^{-1}.min^{-1}$)	0.003903	0.002027	0.002276	0.002077	0.003109
$Q_{m\ (cal)}$ (mg/g)	11.82	20.79	23.36	32.79	18.98
$Q_{m\ (exp)}$ (mg/g)	10.67	18.19	21.05	21.90	18.12

Table 3. 7**:** The kinetic parameters for adsorption DCF using Fe^0-PG composite of the pseudo-second-order linear fits using equations 6 and 8 at different concentrations at 298K.

Ho Equation	**20 mg/L**	**25 mg/L**	**30 mg/L**	**35mg/L**	**45 mg/L**
Slope	0.0497	0.0344	0.033	0.0305	0.0252
R^2	0.9976	0.992	0.9885	0.9985	0.9997
Intercept	0.8902	1.2259	1.0378	0.7766	0.5183
k_2 $(g.mg^{-1}.min^{-1})$	0.002775	0.0009653	0.001049	0.001198	0.001225
$Q_{e\,(cal)}$ (mg/g)	20.12	29.07	30.30	32.79	39.68
$Q_{e\,(exp)}$ (mg/g)	18.38	25.05	26.36	29.03	35.71
Shahwan Equation					
Slope	0.0497	0.0344	0.033	0.0305	0.0252
R^2	0.9976	0.992	0.9885	0.9985	0.9997
Intercept	0.8902	1.2259	1.0378	0.7766	0.5183
k_2 $(L.mg^{-1}.min^{-1})$	0.003	0.0011482	0.001157	0.001179	0.001225
$Q_{m\,(cal)}$ (mg/g)	20.12	29.07	30.30	32.79	39.68
$Q_{m\,(exp)}$ (mg/g)	18.38	25.05	26.36	29.03	35.71

From Table 3.6 and Table 3.7. Shahwan equation shows a higher rate constant of removal of DCF by Fe^0 NPs than the rate constant of removal of DCF Fe^0-PG composite, so the removal process by Fe^0 NPs is faster than Fe^0-PG composite.

To check which of the two equations gives a closer correlation with the experimental results the calculated k_2 and Q values were entered in the nonlinear equations (5 and 7), then the model prediction was obtained from the calculated Q values. After that, a plot of experimental and predicted data of Q versus time for two types of adsorbent were obtained as shown in Figure 3.11 and Figure 3.12.

In Figure 3.11(a) and Figure 3.12 (a), for Fe^0 NPs the correlation is preferable at all concentrations in the two models.

On the other hand, Figure 3.11(b) and Figure 3.12 (b), for Fe^0-PG composite the two models showed similar correlation, both models fitted to the experimental data at all concentrations

.

a

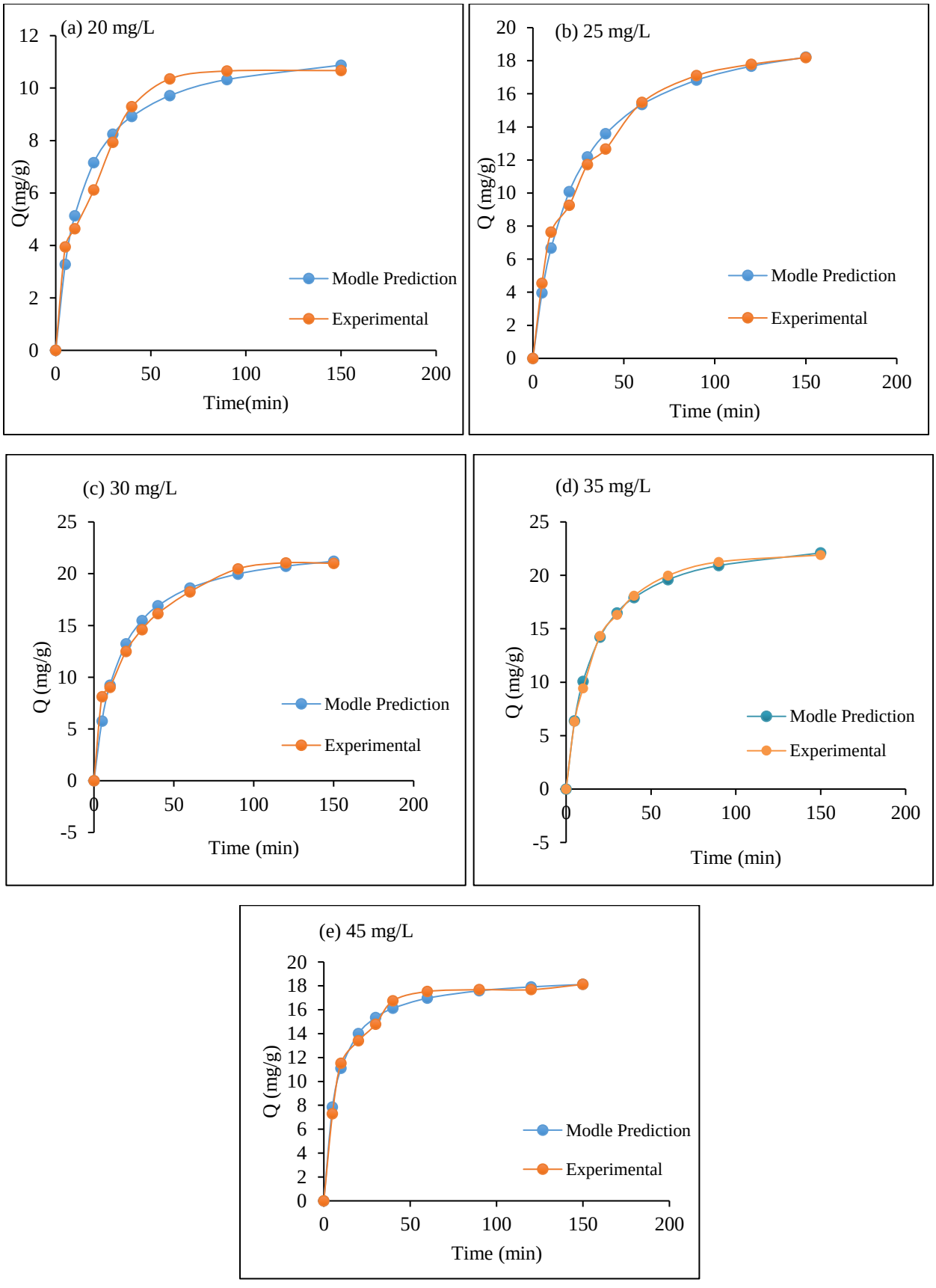
(a) 20 mg/L
Q(mg/g)
Time(min)
Modle Prediction
Experimental
(b) 25 mg/L
Q (mg/g)
Time (min)
Modle Prediction
Experimental
(c) 30 mg/L
Q (mg/g)
Time (min)
Modle Prediction
Experimental
(d) 35 mg/L
Q (mg/g)
Time (min)
Modle Prediction
Experimental
(e) 45 mg/L
Q (mg/g)
Time (min)
Modle Prediction
Experimental

b

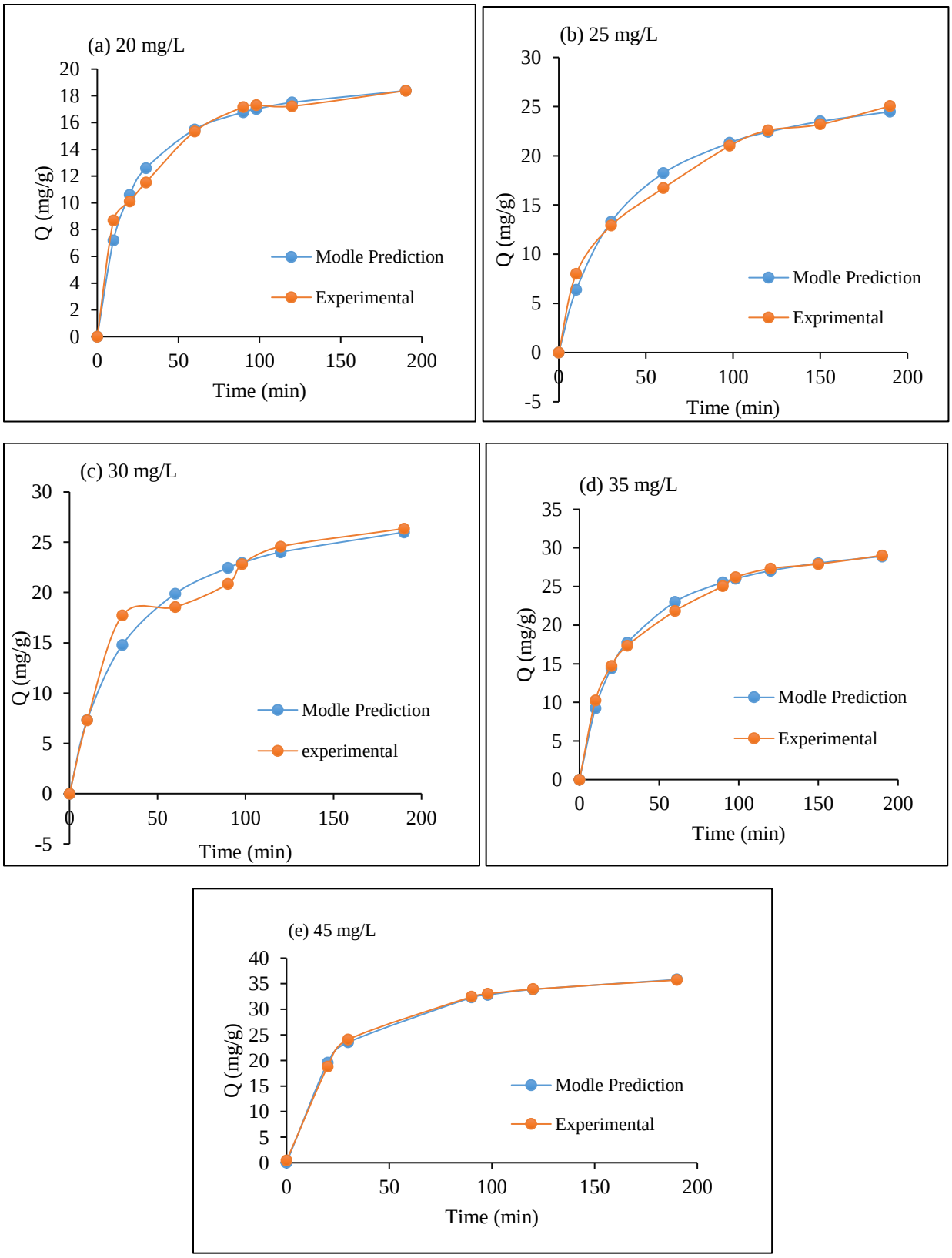

Figure 3. 11: Nonlinear fits of the kinetic data of DCF removal via a) Fe^0 NPs and b) Fe^0-PG composite using Ho equation.

a

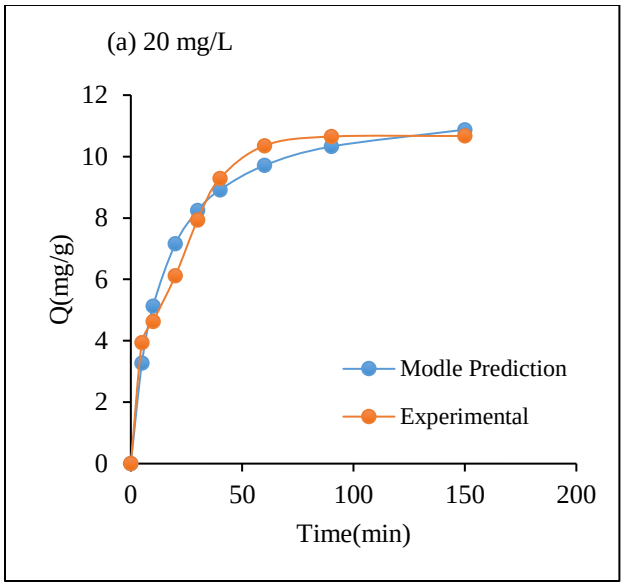
(a) 20 mg/L
Q(mg/g)
Time(min)
Modle Prediction
Experimental

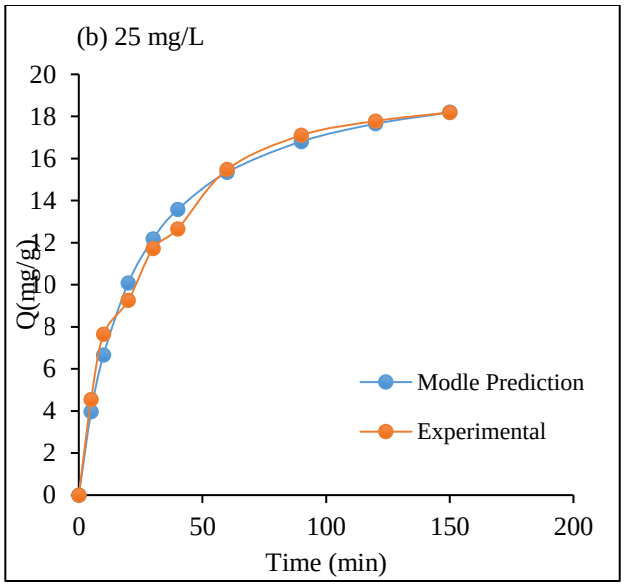
(b) 25 mg/L
Q(mg/g)
Time (min)
Modle Prediction
Experimental

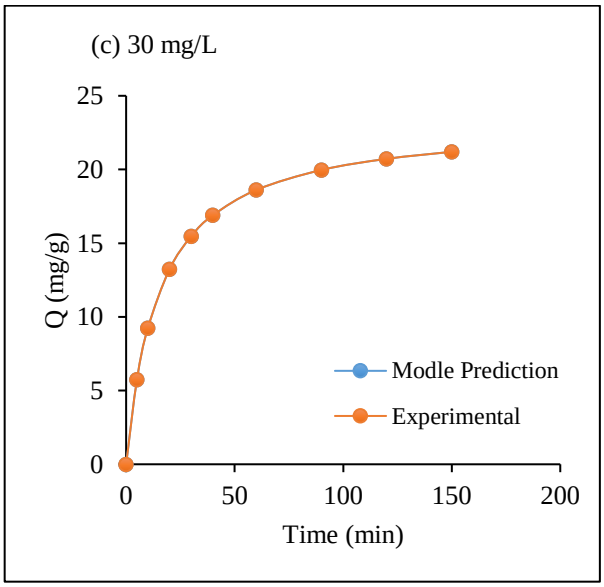
(c) 30 mg/L
Q (mg/g)
Time (min)
Modle Prediction
Experimental

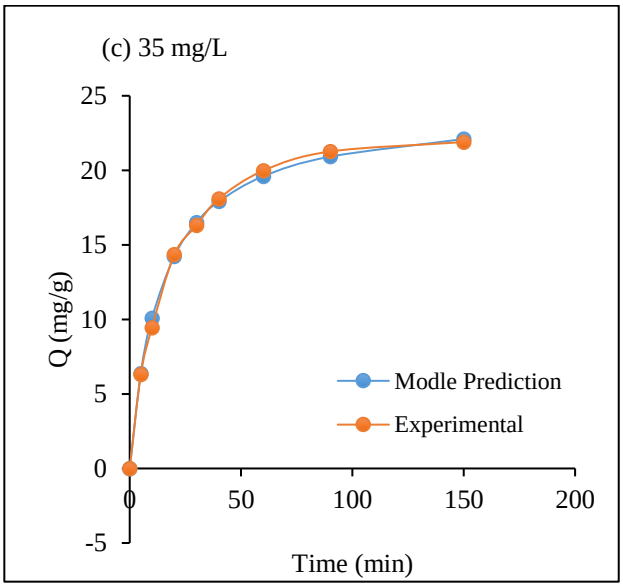
(c) 35 mg/L
Q (mg/g)
Time (min)
Modle Prediction
Experimental

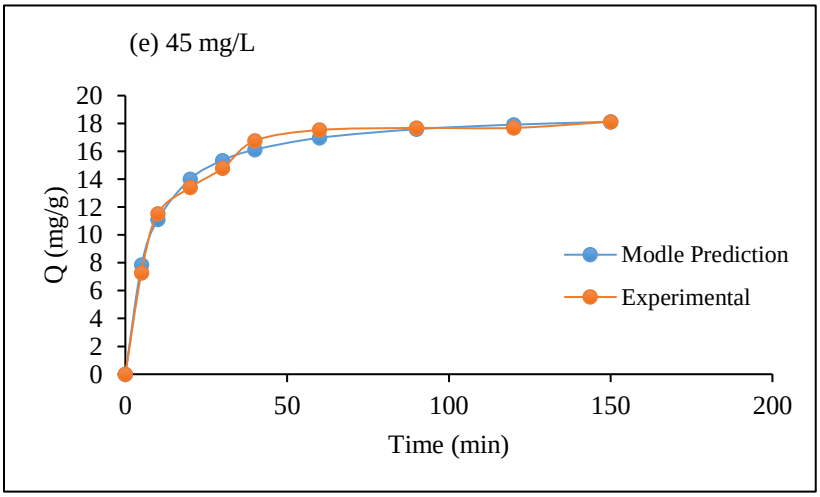
(e) 45 mg/L
Q (mg/g)
Time (min)
Modle Prediction
Experimental

b

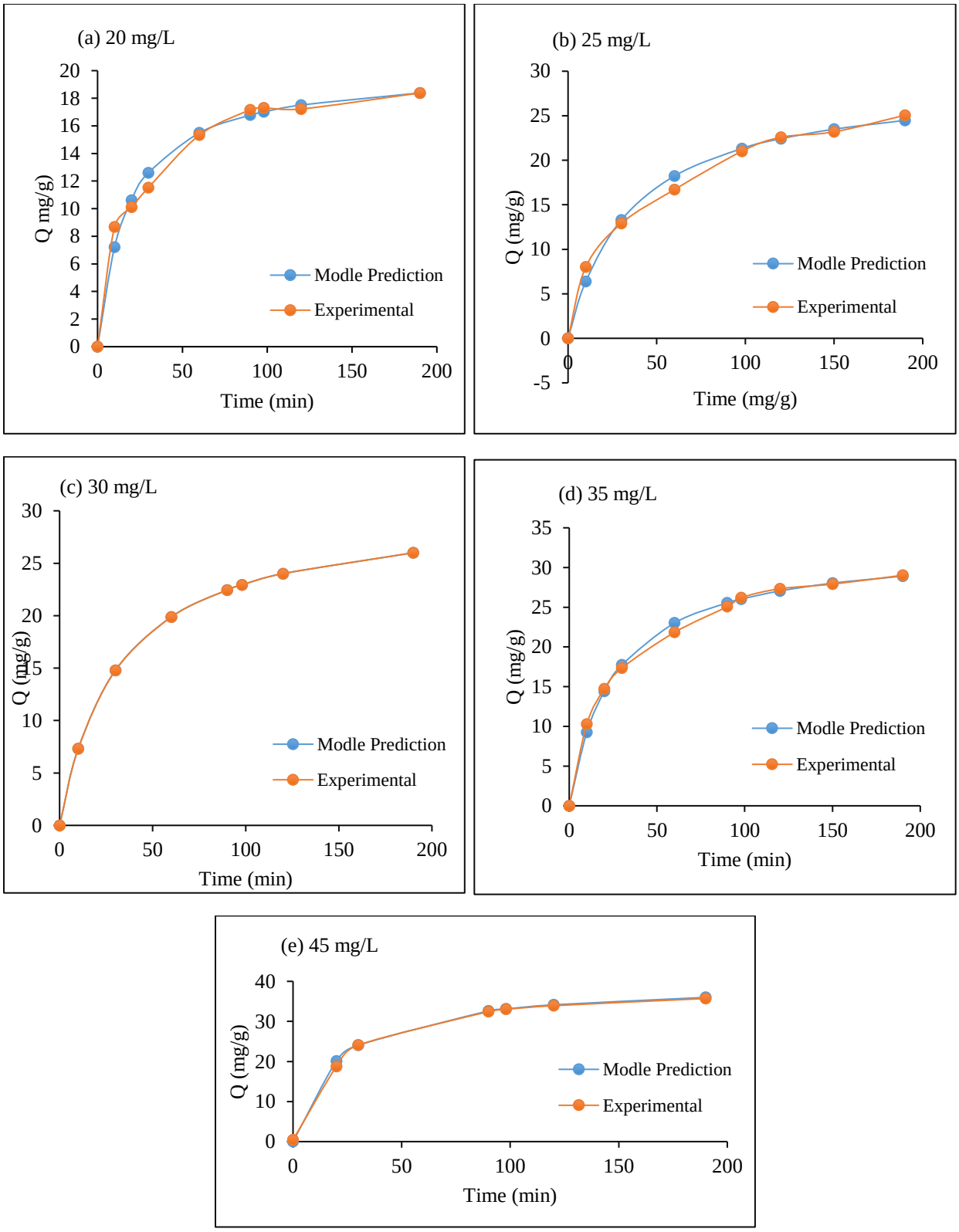

Figure 3. 12: Nonlinear fits of the kinetic data of DCF removal by a) Fe^0 NPs and b) Fe^0-PG composite using Shahwan equation.

As a further test of the correlation, the Chi test was performed to estimate the difference between experimental values and predicted using non-linear forms equation (5) and equation (7). The following equation was used to calculate the Chi-square values:

$$\chi^2 = \sum_{1}^{n} \frac{(Q_{exp} - Q_{pred})^2}{Q_{pred}} \dots\dots\dots\dots\dots\dots\dots\dots (9)$$

The smaller values of ($\boldsymbol{\chi^2}$) means that the difference between experimental and predicted values is smaller. Table 3.8 and Table 3.9 show the values of $\boldsymbol{\chi^2}$ for two models of Ho and Shahwan using Fe^0 NPs and Fe^0-PG composite, Table 3.8 and Table 3.9 show that the Chi test provides similar values at all concentrations. This confirms that the non-linear pseudo-second-order model and Shahwan model are similar in describing the adsorption kinetic process for both adsorbents.

Table 3. 8**:** The Chi–test values of Ho model for Fe^0 NPs and Fe^0-PG composite using equation (9) at different concentrations.

C_0 (mg/L)	**Chi-test (χ^2) Ho model**	
	Fe^0 NPs	Fe^0-PG composite
20	0.4180	0.4379
25	0.3842	0.5841
30	1.128	0.7987
35	0.06238	0.2027
45	0.1508	0.04698

Table 3. 9**:** The Chi–test values of Shahwan model for Fe^0 NPs and Fe^0-PG composite using equation (9) at different concentrations.

C_0 (mg/L)	**Chi-test (χ^2) Shahwan model**	
	Fe^0 NPs	Fe^0-PG composite
20	0.418	0.4364
25	0.3833	0.5841
30	1.128	0.7987
35	0.06251	0.2027
45	0.1508	0.09461

3.4. Effect of Initial DCF Concentration

The effect of DCF concentration was studied at several initial concentrations of DCF: 20, 25, 30, 35, and 45 mg/L for the two types of NPs at 298K. The percentage removal equation was used to calculate the % removal of DCF as shown in Figure 3.13.

The results of the two NPs indicate that DCF was adsorbed at both low and high concentrations until the adsorbent sites become saturated with time. Thus, the removal extent of DCF did not increase as increasing the initial concentration because the number of active sites on the surface of Fe^0 NPs and Fe^0-PG composite was limited. So, the % removal of DCF is decreased as concentration increases, but this result was not valid between 20 mg/L and 25mg/L.

The results show, at 25mg/L the % removal of Fe0 NPs and Fe0-PG composite was 61.16% and 95.16% respectively, On the contrary, PG didn't show a significant removal for DFC in aqueous solutions at all concentrations. This result shows that the modification on Fe0 NPs increases its efficiency in the removal of DCF.

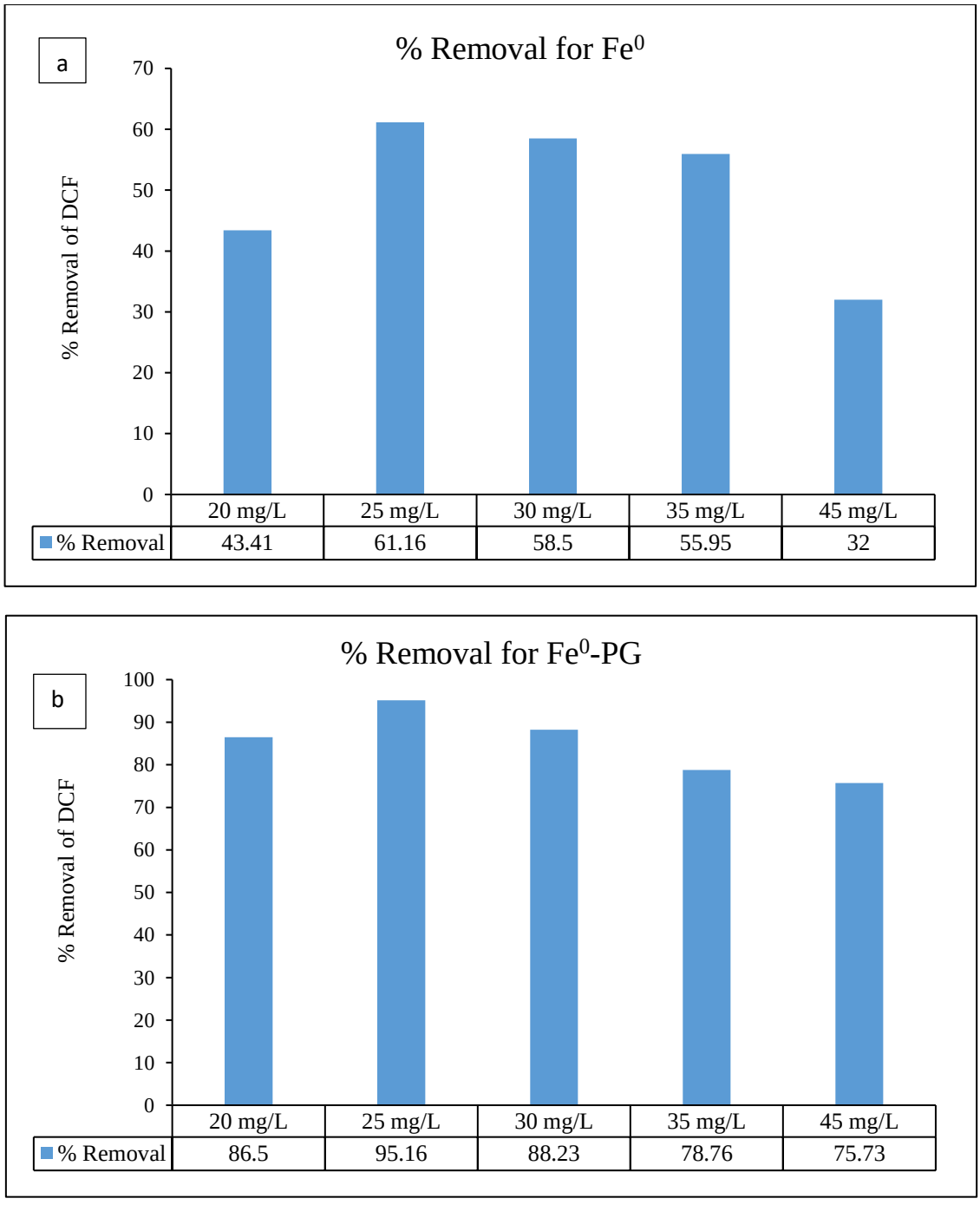

Figure 3. 13: Effect of initial DCF concentration on percentage removal by a) Fe^0 NPs and b) Fe^0-PG composite.

Also, the concentration of DCF on the NPs surface (Q, mg/g) was calculated. From Table 3.10 the Q value increases with increasing the DCF initial concentration for the two types of nanoparticles, but it turns to decrease for Fe^0 NPs at 45 mg/L. Therefore, the highest adsorption capacity for Fe^0-PG composite was obtained at the highest DCF concentration and 35 mg/L for Fe^0 NPs. This means as increase the amount of DCF in the solution, the amount of loded perticals on the surface of NPs increase.

Table 3. 10**:** The calculated Q values of adsorbed DCF onto Fe^0 NPs and Fe^0-PG composite at different initial concentrations.

C_0 (mg/L)	**Q (mg/g)**	
	Fe^0 NPs	Fe^0-PG composite
20	11.82	20.12
25	20.79	29.07
30	23.36	30.30
35	24.15	32.79
45	18.98	39.68

3.5 Adsorption Isotherms

The adsorption isotherms are utilized to model the partitioning of DCF between the solution and the adsorbent, as equilibrium is established. Langmuir and Freundlich isotherms models were employed to understand the sorption mechanism of the adsorbate onto the surface of the adsorbent and the homogeneity of that surface. Langmuir model is well fitted with the monolayer adsorption takes place onto an adsorbent that has a uniform and homogenous surface.[90,91]

The amount of DCF adsorbed by Fe^0 NPs and Fe^0-PG composite at equilibrium, which is represented as q_e (mg/g) was calculated by the mass balance equation given in equation 1.

The linear Langmuir adsorption isotherm was utilized to fit the experimental data as shown in Figure 3.14 by following equation form:

$$\frac{C_e}{Q_e} = \frac{1}{Q_m K_L} + \frac{C_e}{Q_m} \qquad (10)$$

Where C_e is the equilibrium concentration of the DCF solution (mg/L), Q_e is the amount of DCF adsorbed per gram of the adsorbent at equilibrium (mg/g). Q_m is the maximum amount of DCF (mg) adsorbed per gram of adsorbents for complete

monolayer coverage. k_L is the Langmuir constant related to the energy of adsorption (L/mg).

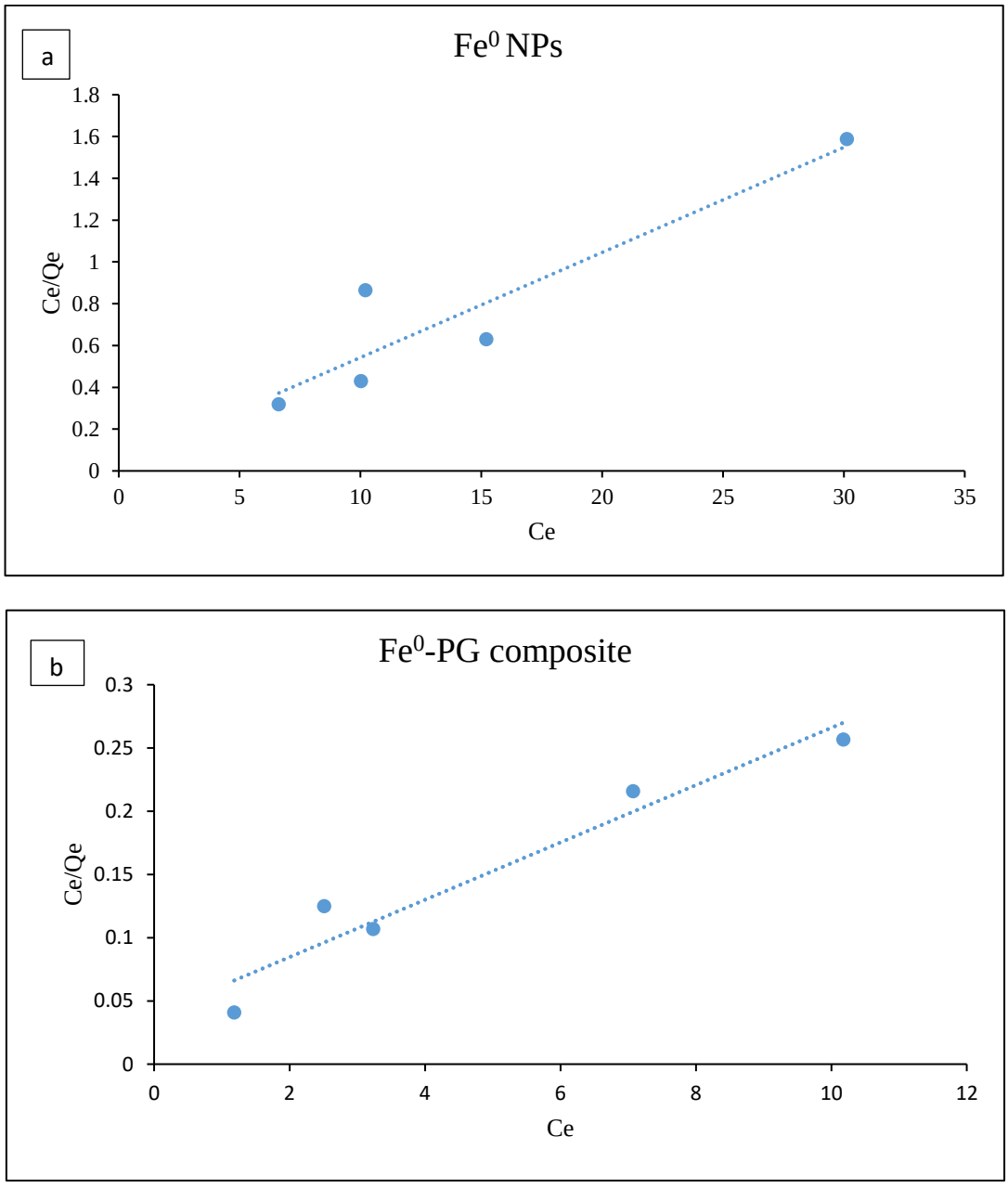

Figure 3. 14: Linear plots of Langmuir isotherm model of DCF adsorption onto a) Fe^0 NPs and b) Fe^0-PG composite at 298K.

Another adsorption model that is widely applied is the Freundlich isotherm, for multilayer adsorption, it is utilized for heterogeneous adsorbent surfaces that have different sites with differing adsorption energy. [92,93] It was also applied to the experimental data for adsorption of DCF onto Fe^0 NPs and Fe^0-PG composite as shown in Figure 3.15.

The nonlinear form of the Freundlich isotherm model is given as:

$$Q_e = k_f \, C_e^{\frac{1}{n}} \qquad (11)$$

The linearized form of the Freundlich isotherm model is represented by this equation:

$$lnQ_e = lnk_f + \left(\frac{1}{n}\right) lnC_e \qquad (12)$$

Where C_e is the equilibrium concentration of the DCF solution (mg/L), and Q_e is the amount of DCF adsorbed per gram of the adsorbent at equilibrium (mg/g). k_f is the Freundlich constant, which reflects the adsorption affinity, and n is the Freundlich constant related to the adsorption linearity.

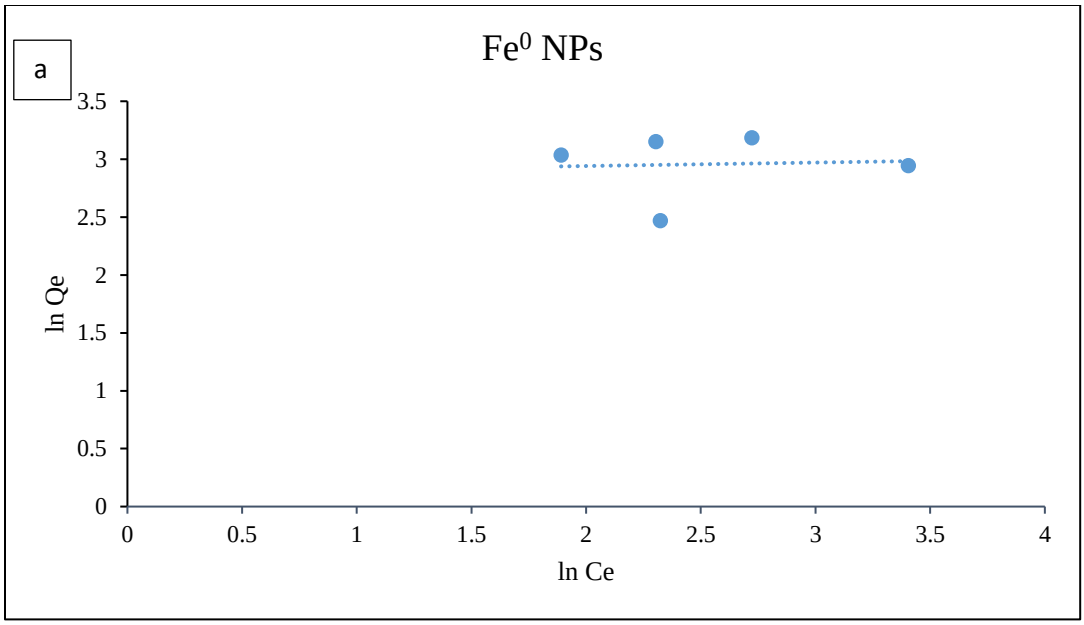

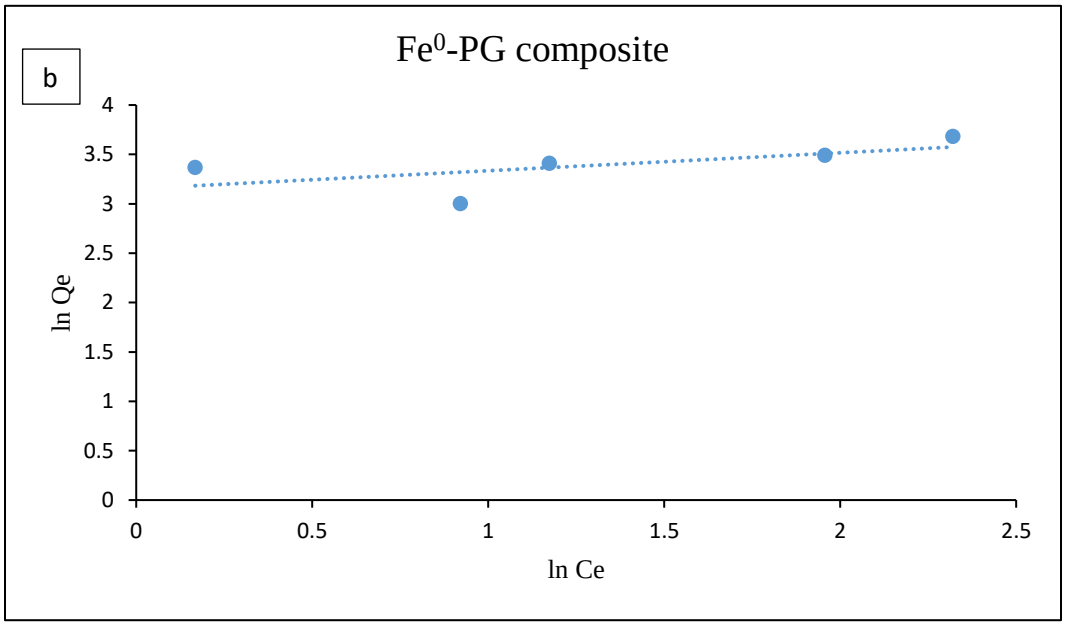

Figure 3. 15: Linear plots of Freundlich isotherm model of DCF adsorption via a) Fe^0 NPs and b) Fe^0-PG composite at 298K.

The parameters for the Langmuir and Freundlich models of Fe^0 NPs and Fe^0-PG composite were calculated and listed in Table 3.11 at 25mg/L of DCF at 298K.

The R^2 values of the two NPs in the Langmuir model are higher and better than the Freundlich model that has a low value of R^2, so the adsorption of DCF onto Fe^0 NPs and Fe^0-PG composite is better described by Langmuir isotherm model than Freundlich isotherm model, this indicated that the adsorption of DCF on the surface of Fe^0 NPs and Fe^0-PG composite seems to be monolayer and homogeneous rather than heterogeneous adsorption.

The maximum adsorption capacity of DCF Q_{max} (mg/g) by Fe^0 NPs and Fe^0-PG composite was 19.9, 44.0 respectively. So, the maximum adsorption capacity of the DCF using Fe^0-PG composite is more than Fe^0 NPs. These results indicate that Fe^0-PG composite has higher removal efficiency than Fe^0 NPs. This improvement is attributable to decreasing the aggregation and increasing the surface area of adsorption for Fe^0 NPs in the composite.

Table 3. 11**:** Parameters of Langmuir and Freundlich models for DCF adsorption using Fe^0 NPs and Fe^0-PG composite at 25 mg/L of DCF at 298 K.

	Langmuir			**Freundlich**		
Experimental condition	Q_{max} (mg/g)	k_L (L/mg)	R^2	k_f (L/mg)	n	R^2
Fe^0 NPs	19.9	1.267	0.8583	17.83	33.4	0.0035
Fe^0-PG composite	44.0	0.5776	0.9355	23.40	5.50	0.3912

Table 3.11 summarizes a comparison of the maximum capacities of DCF by different adsorbents including Fe^0 NPs and Fe^0-PG composite for the present study. The comparison indicating that the suitability and applicability of the Fe^0 NPs and Fe^0-PG composite used as an efficient adsorbent for removal of the DCF.

Table 3. 12**:** Maximum adsorption capacities of DCF for different adsorbents.

Adsorbents	**Adsorption capacity (mg/g)**	**References**
Organoclays (Spectroger type C)	9.85	(11)
Cocoa shell activated carbon	63.47	(1)
Powdered activated carbon	233.4	(1)
Activated carbon with $ZnCl_2$	156.7	(12)
reduced graphene oxide(rGO)	59.67	(13)
Fe^0 NPs	19.9	This study
Fe^0-PG composite	44.0	This study

3.6 Effect of pH and PZC on the Removal of DCF

One of the important parameters that affect the adsorption of DCF by Fe^0-PG composite is the pH. The effect of pH on the removal of DCF was studied at pH values ranging from 4 to 9. The pH of the solution was changed by using 0.1M NaOH and 0.1M HCl solutions.

Figure 3.16 shows the effects of the pH on the % removal of DCF, it is clear that the adsorption of DCF increase from pH= 4 to pH= 6 due to increase the % removal of DCF from 22.6% to 83.5%, then decreases as pH values increases from 6 to 9. These values depend on several things: the morphology of the adsorbent change, the charge on its surface, and the degree of dissociation for the adsorbate.

The point of zero charge (pH_{pzc}) gives information about the charges of the outer surface of the particle. PZC is the pH at which the net surface charge of the material (positive and negative charges) are equivalent. The effect of PZC on the removal of DCF was determined by the salt addition method at pH values ranging from 2-11 as shown in Figure 3.17.

The results obtained show that the PZC was around 6.0, and the net charge on the surface of Fe^0-PG was positive when $pH < pH_{PZC}$, and negative in a range of $pH > pH_{PZC}$.

Depending on the Electrostatic attraction forces, the pH decreases, as available protons increase, they induce the formation of Fe(II)-DCF complex or hydrogen bond by the positive ionization of Fe^0-PG surface and de-protonation of DCF (-COO-). DCF is a weak acid (pKa =4.0), at pH > 4.0 DCF surface is negatively charged due to de-protonation and the net charge

of the Fe^0-PG surface is positive until pH =6.0. Therefore, the high adsorption capacity at the pH ranged from (2.0–6.0) was because of the high electrostatic attraction between the DCF and Fe^0-PG composite. At pH >6.0, the adsorption capacity decreases as pH values increase due to the repulsion forces between the negative charges in the DCF and Fe^0-PG composite surface. Moreover, other reasons that could decrease the adsorption efficiency at high pH values are the precipitation and the formation of iron oxide. It was observed that the precipitation of DCF from the solution was at a pH less than its pKa. Also, the presence of hydroxide ions cause clogging of the active sites on the Fe^0-PG composite surface by forming shells around Fe^0-PG composite particles.[94]

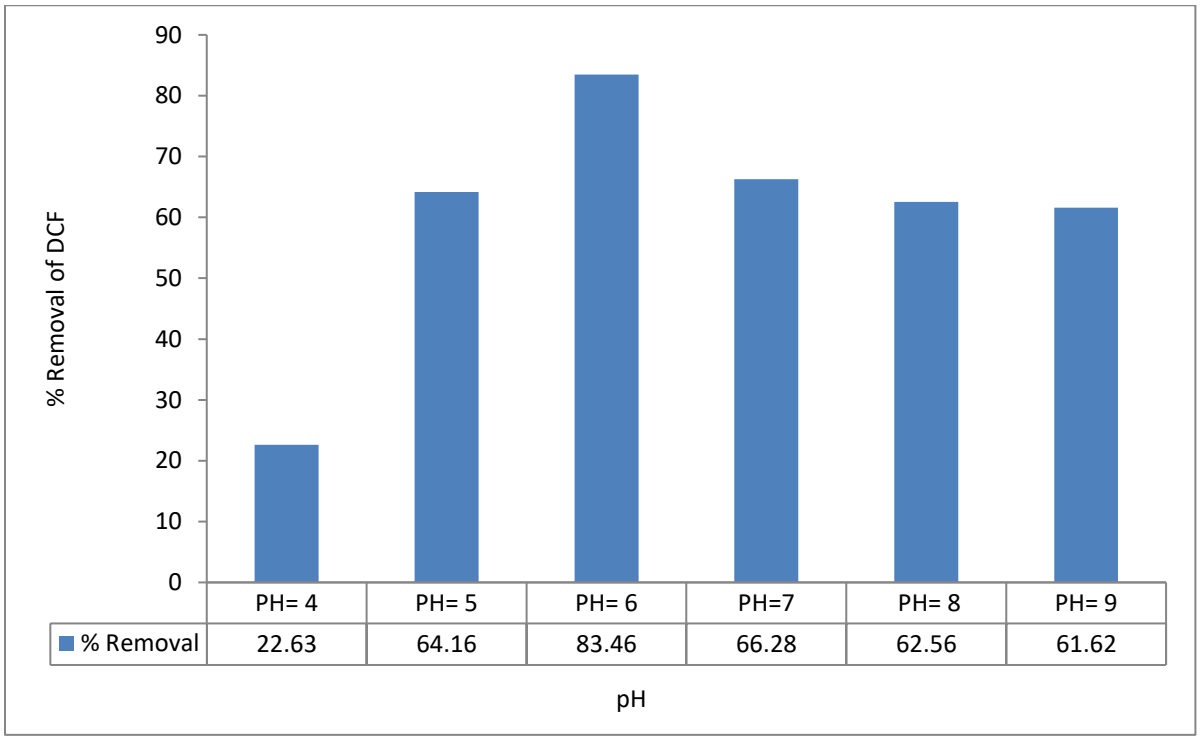

Figure 3. 16: Effect of pH on the percentage removal of DCF using Fe^0-PG composite at 298K.

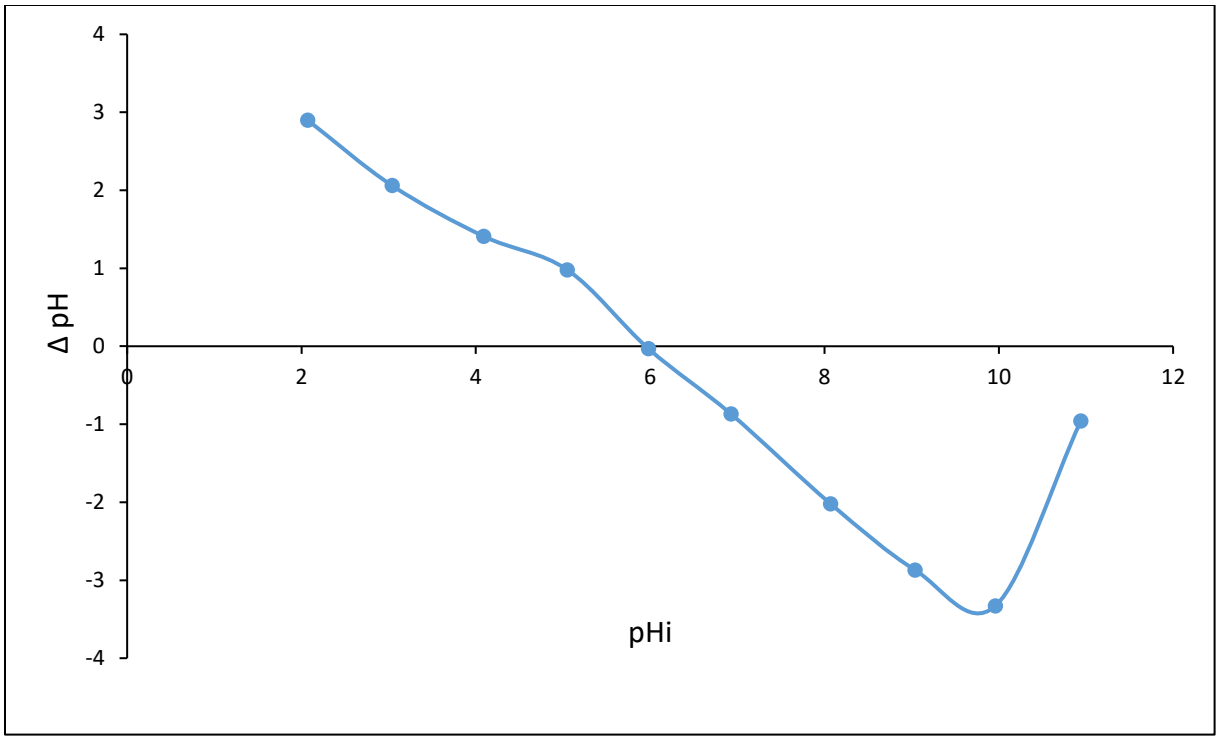

Figure 3. 17: Evaluation of pH_{pzc} for Fe^0-PG composite at 298K.

3.7 Effect of Temperature

The effect of temperature on the adsorption of DCF process was studied using Fe^0 NPs and Fe^0-PG composite and 25mg/L of DCF at different temperatures: 283, 288, 298, and 308K.

The activation energy of adsorption of DCF on Fe^0 NPs and Fe^0-PG composite was calculated from the kinetics data obtained at different temperatures as shown in Figure 3.19 using the Arrhenius equation: [95]

$$\ln k_2 = \ln A - \frac{E_a}{R\,T}. \quad (13)$$

Where k_2 is the rate constant of pseudo-second-order (g mg^{-1} min^{-1}).

A is the pre-exponential factor.

E_a is the activation energy (kJ mol^{-1}).

R is the gas constant (8.314 J K^{-1} mol^{-1}).

T is the absolute temperature (K).

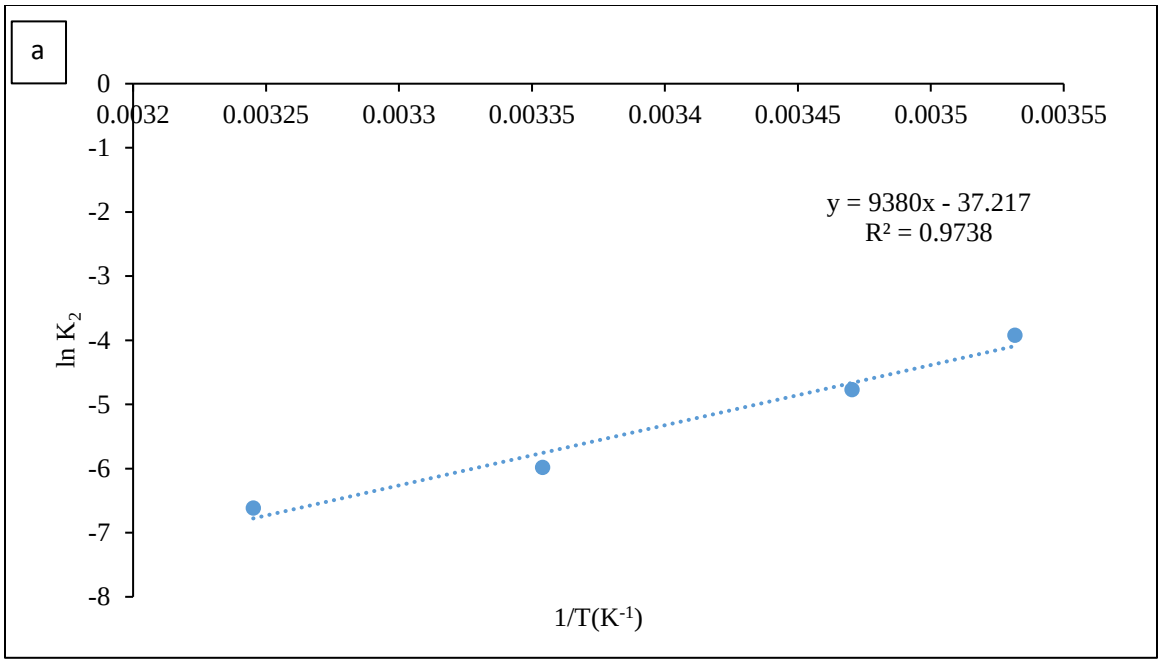

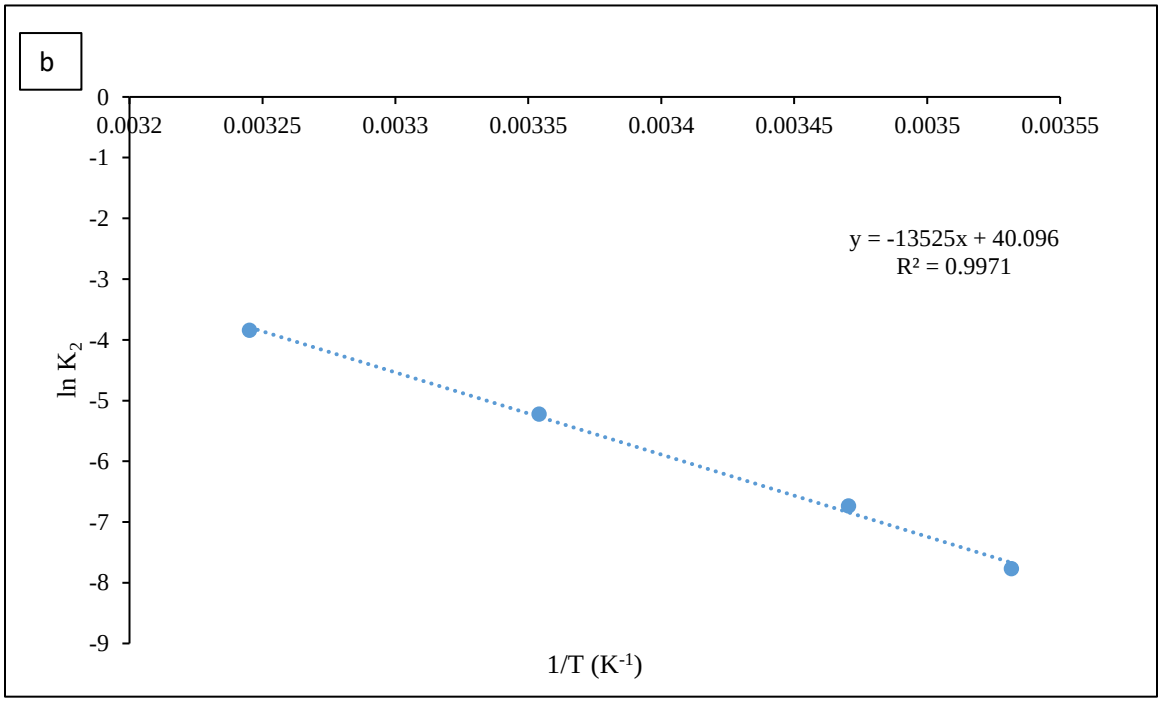

Figure 3. 18: Arrhenius equation graph of DCF adsorption for a) Fe^0 NPs and b) Fe^0-PG composite.

The activation energy values predict if the adsorption mechanism is physisorption (from 5-40 kJ mol^{-1}) or chemisorption (from 40 to 800 kJ mol^{-1}).[96]

As shown in Table 3.13 the magnitude of the activation energy barrier for adsorption of DCF onto Fe^0-PG composite was calculated to be 112 (kJ mol^{-1}) meaning that the adsorption mechanism is chemisorption, while the magnitude of activation energy barrier in adsorption of DCF onto Fe^0 NPs was calculated to be -78.0 (KJ mol^{-1}), one of the accepted explanations for this result is a multistep reactions which have apparent negative activation energies. This means the overall rate constant K for a two-step reaction $A \rightleftharpoons B$, $B \rightarrow C$ is represented as $K = k_2k_1$, where k_2 is the rate constant for the slow second step that is limiting the reaction rate and $k_1$is the equilibrium constant of the rapid first step. In this reaction, k_1 decreases with temperature faster than k_2 increases, so the overall k decreases with temperature and a negative activation energy observed.[97] The mathematical negative activation energy for this type of adsorption is expected when $(E_{a,a'} > E_{a,a} + E_{a,b'})$, therefore, $k_r = \frac{k_a k_b}{k_{a'}}$ will decrease upon increasing temperature and the reaction will move slowly to the product as the temperature increased.[98]

Table 3. 13**:** Activation energy and rate constant values of adsorbed DCF onto Fe^0 NPs and Fe^0-PG composite at different temperatures.

	Fe^0 NPs	Fe^0-PG composite
Ea (kJ mol $^{-1}$)	-78.0	112

From Figure 3.19 it seems that the increase in the temperature affects positively the adsorption process, so as temperature increases the adsorption capacity increase. This confirms that the increase of temperature makes stabilization of the physical forces between DCF and adsorbent. Therefore, the amounts of DCF sorption on both nanoparticles increase at the highest temperature because of the change in the equilibrium toward adsorption. [96]

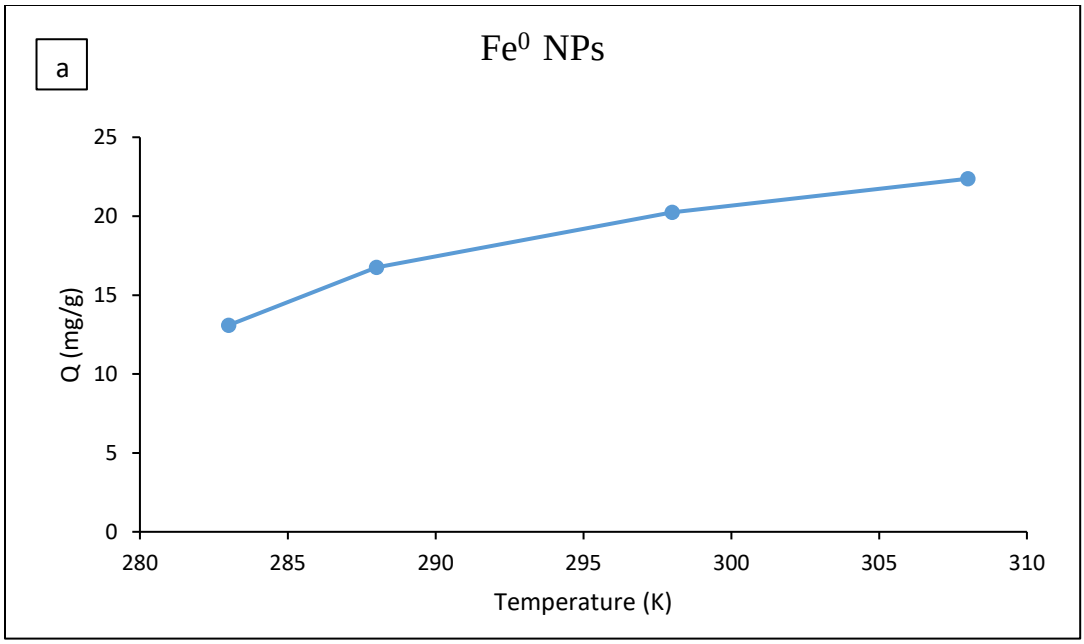

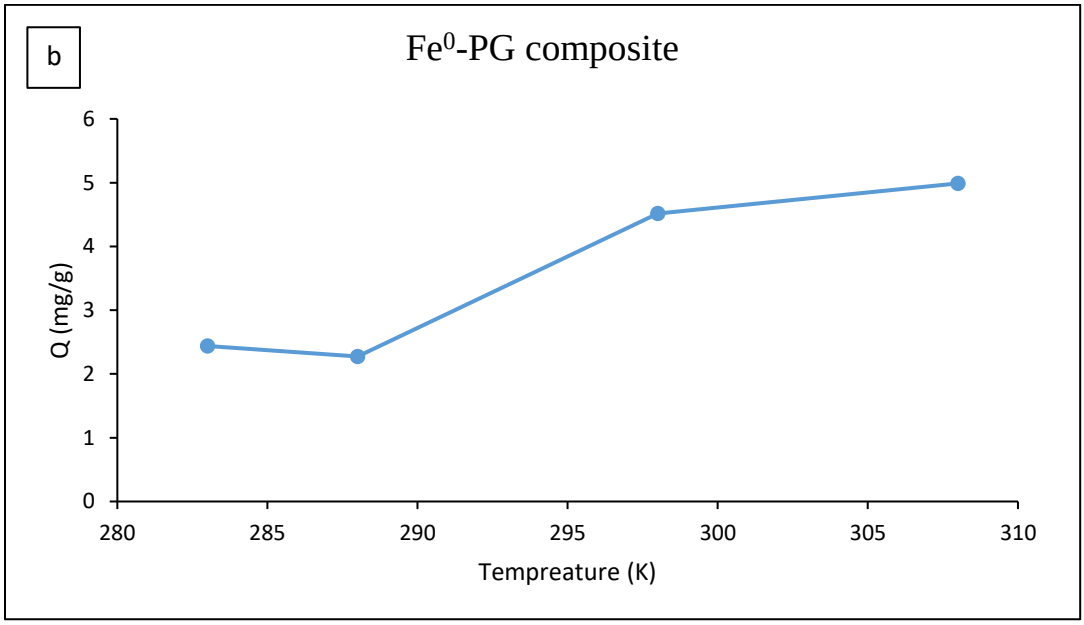

Figure 3. 19: Effect of temperature on the adsorption of DCF onto: a) Fe^0 NPs b) Fe^0-PG composite at 298K.

3.8 Adsorption Thermodynamics

The data obtained from the previous section were analyzed to determine the thermodynamic parameters which are Gibbs free energy change (ΔG°), change in standard enthalpy (ΔH°), and change in standard entropy (ΔS°).

The ΔH° and ΔS° values were obtained using van't Hoff equation: [96]

$$\ln K = \frac{\Delta S^\circ}{R} - \frac{\Delta H^\circ}{R\,T} \qquad (14)$$

The value of Gibbs free energy change (ΔG°) was obtained from the following equations:

$$\Delta G^\circ = \Delta H^\circ - T\,\Delta S^\circ \qquad (15)$$

$$\Delta G^\circ = -RT\,lnK \qquad (16)$$

Where ΔG° change in Gibbs free energy (kJ mol^{-1}), ΔH° change in enthalpy (kJ mol^{-1}), ΔS° change in entropy (kJ mol^{-1} K^{-1}), R is the ideal gas constant (8.3145 J/mol K), T is the temperature in Kelvin, K is the apparent equilibrium constant expressed as $\left(\frac{Q_e}{C_e}\right)$.

The values of ΔH° and ΔS° were calculated from the slope and y-intercept obtained from the linear plot of In $\left(\frac{Q_e}{C_e}\right)$ versus 1/T as shown in Figure 3.20.

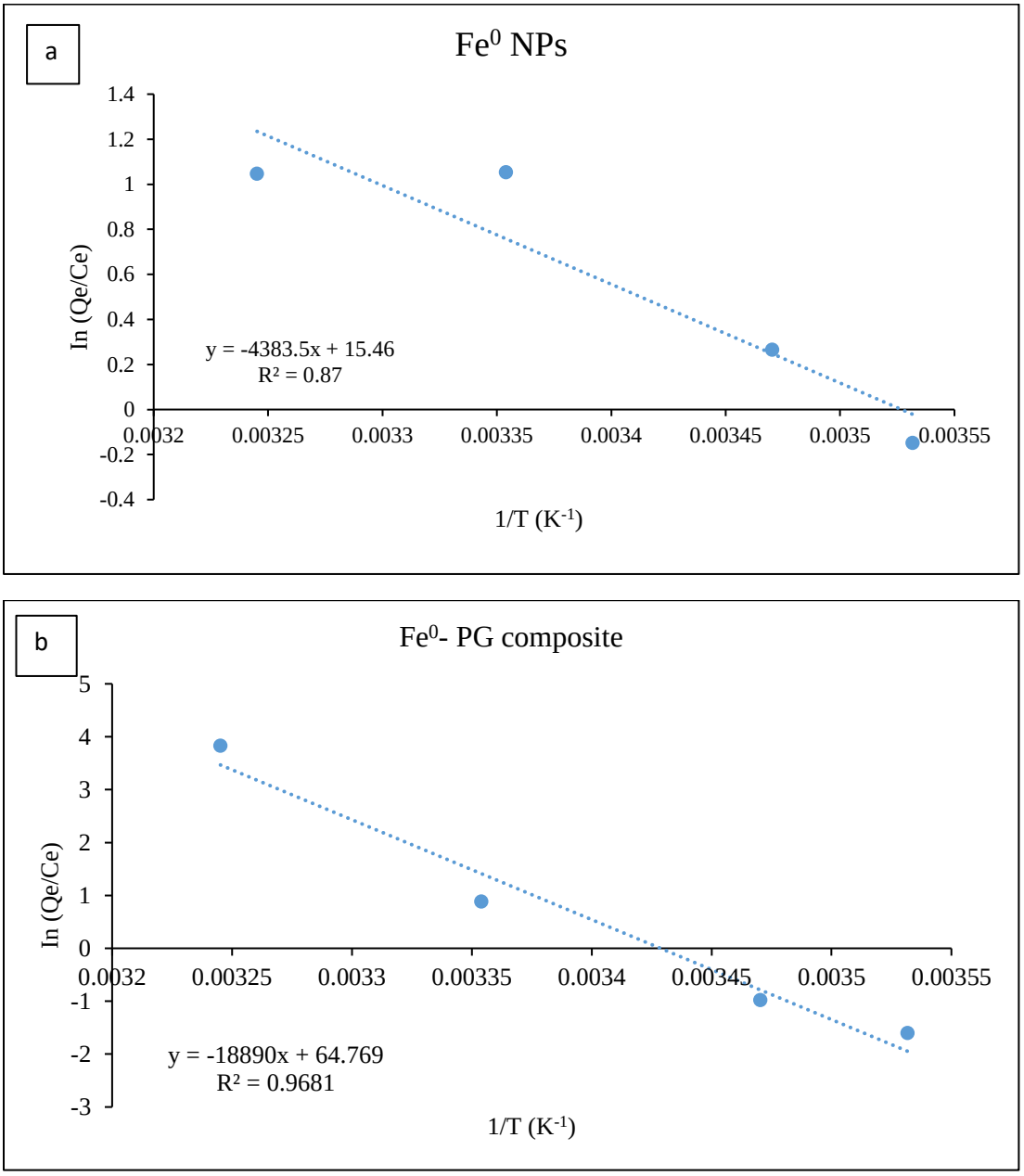

Figure 3. 20: Determination of thermodynamic parameters of DCF adsorbed onto: a) Fe^0 NPs and b) Fe^0-PG composite.

The thermodynamic parameters were calculated and listed in Table 3.14and Table 3.15.

Table 3. 14**:** Thermodynamic parameters of DCF adsorbed using Fe^0 NPs.

ΔH^o (kJ/mol)	ΔS^o (kJ/mol.K)	ΔG^o (kJ/mol)			
		283 K	288 K	298 K	308 K
36.4	0.128	0.050	-0.593	-1.88	-3.16

Table 3. 15**:** Thermodynamic parameters of DCF adsorbed using Fe^0-PG composite.

ΔH^o (kJ/mol)	ΔS^o (kJ/mol.K)	ΔG^o (kJ/mol)			
		283 K	288 K	298 K	308 K
157	0.538	4.57	1.88	-3.51	-8.89

In general, Gibbs free energy (ΔG) represent the driving force of the reaction which could be pontaneous when G is decreasing ($\Delta G < 0$). Under constant pressure conditions and temperature, when G of the reaction goes to minimum ($\Delta G = 0$), then thermodynamic equilibrium is established. This case is useful for closed systems for homogeneous or heterogeneous systems.[99] Negative value of Gibbs free energy (ΔG°) means that the adsorption process favors the products, also the type of adsorption can be

known by its value, if the value of ΔG° in the range from -20 to 0 kJ mol^{-1} it considered a physisorption process, while if the values range from -80 to -400 kJ mol^{-1} it considered a chemisorption process.[100,101]

The value of ΔH°provides information about the type of adsorption if it is in the range 2.1 to 20.9 kJ mol^{-1} and 80 to 200 kJ mol^{-1} it is Physical and chemical adsorption respectively. Also, the value of ΔH° of the adsorption process can be used to determine if the process is exothermic or endothermic.[87,102]

From Table 3.14 and Table 3.15, the adsorption process of DCF is endothermic due to the positive values of ΔHº. In addition, the ΔHº value for Fe^0 NPs indicates that the adsorption process could be physisorption, while the ΔHº value for Fe^0-PG composite indicates that is chemical adsorption. The positive values of ΔS° indicate that the system is more random and more disorderly. Moreover, DCF adsorption was nonspontaneous at 283 K for both NPs and spontaneous at 298K and 308K because ΔGº values were negative at these temperatures.

4. Conclusions

In this study, the Fe^0 NPs and Fe^0-PG composite were synthesized through liquid–reduction method. Then Fe^0 NPs were modified with pencil graphite as a support material.

The adsorption behavior of DCF onto Fe^0 NPs and Fe^0-PG composite surface was studied. It was found that the kinetic data correlates better with the pseudo-second-order equation than with the pseudo-first-order equation. The calculated value of activation energy shows that the Fe^0 NPs have a negative value of activation barrier of DCF sorption while Fe^0-PG composite has positive activation energy. The value of rate constant increases with decreasing the value of activation energy, so the rate constant values for adsorption of DCF onto Fe^0-PG composite are larger than that of the adsorption of DCF onto Fe^0 NPs. Moreover, the maximum adsorption capacities of Fe^0-PG composite are larger than those corresponding to Fe^0 NPs.

The concentration and pH both affected the adsorption of DCF using Fe^0 NPs and Fe^0-PG composite. The removal efficiency of DCF from aqueous solution increases till pH values reached 6 then becoming decreases. On the other hand, the amount of DCF adsorbed increases with the decrease the initial concentration of DCF.

In addition, the temperature change affects the extent of the DCF removal process; the increase in temperature leads to an increase in the adsorbed amount of DCF at a specific concentration.

Finally, thermodynamic results indicate that the adsorption of DCF via both Fe^0 NPs and Fe^0-PG composite is endothermic in both cases.

5. References

1. Bishoge, O. K.; Zhang, L.; Suntu, S. L.; Jin, H.; Zewde, A. A.; Qi, Z., Remediation of water and wastewater by using engineered nanomaterials: a review. *Journal of Environmental Science and Health, Part A* **2018,** *53* (6), 537-554.

2. Charradi, K.; Ahmed, Z.; BenMoussa, M. A.; Beji, Z.; Brahmia, A.; Othman, I.; Haija, M. A.; Chtourou, R.; Keshk, S. M., A facile approach for the synthesis of spinel zinc ferrite/cellulose as an effective photocatalyst for the degradation of methylene blue in aqueous solution. *Cellulose* **2022**, 1-12.

3. Ladu, J. L. C.; Athiba, A. L.; Lako, S. T. V.; Alfred, M. L., Investigation on the impact of water pollution on human health in Juba County, Republic of South Sudan. *Journal of Environment Pollution and Human Health* **2018,** *6* (3), 89-95.

4. Yunus, I. S.; Harwin; Kurniawan, A.; Adityawarman, D.; Indarto, A., Nanotechnologies in water and air pollution treatment. *Environmental Technology Reviews* **2012,** *1* (1), 136-148.

5. Haseena, M.; Malik, M. F.; Javed, A.; Arshad, S.; Asif, N.; Zulfiqar, S.; Hanif, J., Water pollution and human health. *Environmental Risk Assessment and Remediation* **2017,** *1* (3).

6. Bartolomeu, M.; Neves, M.; Faustino, M.; Almeida, A., Wastewater chemical contaminants: Remediation by advanced oxidation processes. *Photochemical & Photobiological Sciences* **2018,** *17* (11), 1573-1598.

7. dos Reis, G. S.; Mahbub, M. K. B.; Wilhelm, M.; Lima, E. C.; Sampaio, C. H.; Saucier, C.; Dias, S. L. P., Activated carbon from sewage sludge for removal of sodium diclofenac and

nimesulide from aqueous solutions. *Korean Journal of Chemical Engineering* **2016,** *33* (11), 3149-3161.

8. Tambosi, J. L.; Yamanaka, L. Y.; José, H. J.; Moreira, R. d. F. P. M.; Schröder, H. F., Recent research data on the removal of pharmaceuticals from sewage treatment plants (STP). *Química Nova* **2010,** *33* (2), 411-420.

9. Cunningham, V. L.; Binks, S. P.; Olson, M. J., Human health risk assessment from the presence of human pharmaceuticals in the aquatic environment. *Regulatory toxicology and pharmacology* **2009,** *53* (1), 39-45.

10. Luo, Y.; Guo, W.; Ngo, H. H.; Nghiem, L. D.; Hai, F. I.; Zhang, J.; Liang, S.; Wang, X. C., A review on the occurrence of micropollutants in the aquatic environment and their fate and removal during wastewater treatment. *Science of the total environment* **2014,** *473*, 619-641.

11. Deblonde, T.; Cossu-Leguille, C.; Hartemann, P., Emerging pollutants in wastewater: a review of the literature. *International journal of hygiene and environmental health* **2011,** *214* (6), 442-448.

12. Geissen, V.; Mol, H.; Klumpp, E.; Umlauf, G.; Nadal, M.; Van der Ploeg, M.; Van de Zee, S. E.; Ritsema, C. J., Emerging pollutants in the environment: a challenge for water resource management. *International soil and water conservation research* **2015,** *3* (1), 57-65.

13. de Andrade, J. R.; Oliveira, M. F.; da Silva, M. G.; Vieira, M. G., Adsorption of pharmaceuticals from water and wastewater using nonconventional low-cost materials: a review. *Industrial & Engineering Chemistry Research* **2018,** *57* (9), 3103-3127.

14. Frost, R. L.; Xi, Y.; He, H., Synthesis, characterization of palygorskite supported zero-valent iron and its application for methylene blue adsorption. *Journal of colloid and interface science* **2010,** *341* (1), 153-161.

15. Schwarzenbach, R. P.; Egli, T.; Hofstetter, T. B.; Von Gunten, U.; Wehrli, B., Global water pollution and human health. *Annual review of environment and resources* **2010,** *35*, 109-136.

16. Yang, X.; Flowers, R. C.; Weinberg, H. S.; Singer, P. C., Occurrence and removal of pharmaceuticals and personal care products (PPCPs) in an advanced wastewater reclamation plant. *Water research* **2011,** *45* (16), 5218-5228.

17. Fazal, S.; Zhang, B.; Zhong, Z.; Gao, L.; Chen, X., Industrial wastewater treatment by using MBR (membrane bioreactor) review study. *Journal of Environmental Protection* **2015,** *6* (06), 584.

18. Verma, A. K.; Dash, R. R.; Bhunia, P., A review on chemical coagulation/flocculation technologies for removal of colour from textile wastewaters. *Journal of environmental management* **2012,** *93* (1), 154-168.

19. Amuda, O.; Alade, A., Coagulation/flocculation process in the treatment of abattoir wastewater. *Desalination* **2006,** *196* (1-3), 22-31.

20. Teh, C. Y.; Budiman, P. M.; Shak, K. P. Y.; Wu, T. Y., Recent advancement of coagulation–flocculation and its application in wastewater treatment. *Industrial & Engineering Chemistry Research* **2016,** *55* (16), 4363-4389.

21. Kobya, M.; Demirbas, E.; Senturk, E.; Ince, M., Adsorption of heavy metal ions from aqueous solutions by activated carbon prepared from apricot stone. *Bioresource technology* **2005,** *96* (13), 1518-1521.

22. Deegan, A.; Shaik, B.; Nolan, K.; Urell, K.; Oelgemöller, M.; Tobin, J.; Morrissey, A., Treatment options for wastewater effluents from pharmaceutical companies. *International Journal of Environmental Science & Technology* **2011,** *8* (3), 649-666.

23. Ikehata, K.; Jodeiri Naghashkar, N.; Gamal El-Din, M., Degradation of aqueous pharmaceuticals by ozonation and advanced oxidation processes: a review. *Ozone: Science and Engineering* **2006,** *28* (6), 353-414.

24. Beijer, K.; Björlenius, B.; Shaik, S.; Lindberg, R. H.; Brunström, B.; Brandt, I., Removal of pharmaceuticals and unspecified contaminants in sewage treatment effluents by activated carbon filtration and ozonation: Evaluation using biomarker responses and chemical analysis. *Chemosphere* **2017,** *176*, 342-351.

25. Ternes, T. A.; Meisenheimer, M.; McDowell, D.; Sacher, F.; Brauch, H.-J.; Haist-Gulde, B.; Preuss, G.; Wilme, U.; Zulei-Seibert, N., Removal of pharmaceuticals during drinking water treatment. *Environmental science & technology* **2002,** *36* (17), 3855-3863.

26. Dialynas, E.; Mantzavinos, D.; Diamadopoulos, E., Advanced treatment of the reverse osmosis concentrate produced during reclamation of municipal wastewater. *Water research* **2008,** *42* (18), 4603-4608.

27. Kurniawan, T. A.; Chan, G. Y.; Lo, W.-H.; Babel, S., Physico–chemical treatment techniques for wastewater laden with heavy metals. *Chemical engineering journal* **2006,** *118* (1-2), 83-98.

28. Radjenović, J.; Petrović, M.; Ventura, F.; Barceló, D., Rejection of pharmaceuticals in nanofiltration and reverse osmosis membrane drinking water treatment. *Water research* **2008,** *42* (14), 3601-3610.

29. Ng, K.-K.; Lin, A. Y.-C.; Yu, T.-H.; Lin, C.-F., Tertiary treatment of pharmaceuticals and personal care products by pretreatment and membrane processes. *aquatic* **2011,** *4* (10), 16.

30. Van Hoof, S.; Hashim, A.; Kordes, A., The effect of ultrafiltration as pretreatment to reverse osmosis in wastewater reuse and seawater desalination applications. *Desalination* **1999,** *124* (1-3), 231-242.

31. Ali, I.; Gupta, V., Advances in water treatment by adsorption technology. *Nature protocols* **2006,** *1* (6), 2661-2667.

32. Bhatnagar, A.; Hogland, W.; Marques, M.; Sillanpää, M., An overview of the modification methods of activated carbon for its water treatment applications. *Chemical Engineering Journal* **2013,** *219*, 499-511.

33. Babel, S.; Kurniawan, T. A., Low-cost adsorbents for heavy metals uptake from contaminated water: a review. *Journal of hazardous materials* **2003,** *97* (1-3), 219-243.

34. Jiang, C.; Cui, S.; Han, Q.; Li, P.; Zhang, Q.; Song, J.; Li, M. In *Study on Application of Activated Carbon in Water Treatment*, IOP Conference Series: Earth and Environmental Science, IOP Publishing: 2019; p 022049.

35. Delgado, N.; Capparelli, A.; Navarro, A.; Marino, D., Pharmaceutical emerging pollutants removal from water using powdered activated carbon: study of kinetics and adsorption equilibrium. *Journal of environmental management* **2019,** *236*, 301-308.

36. Volentiru, E.; Nyári, M.; Szabó, G.; Hórvölgyi, Z.; Mureşan, L. M., Silica sol–gel protective coatings against corrosion of zinc substrates. *Periodica Polytechnica Chemical Engineering* **2014**, 61-66.

37. Qu, X.; Brame, J.; Li, Q.; Alvarez, P. J., Nanotechnology for a safe and sustainable water supply: enabling integrated water treatment and reuse. *Accounts of chemical research* **2013,** *46* (3), 834-843.

38. Theron, J.; Walker, J. A.; Cloete, T. E., Nanotechnology and water treatment: applications and emerging opportunities. *Critical reviews in microbiology* **2008,** *34* (1), 43-69.

39. Sotelo, J. L.; Ovejero, G.; Rodríguez, A.; Álvarez, S.; Galán, J.; García, J., Competitive adsorption studies of caffeine and diclofenac aqueous solutions by activated carbon. *Chemical engineering journal* **2014,** *240*, 443-453.

40. de Luna, M. D. G.; Budianta, W.; Rivera, K. K. P.; Arazo, R. O., Removal of sodium diclofenac from aqueous solution by adsorbents derived from cocoa pod husks. *Journal of environmental chemical engineering* **2017,** *5* (2), 1465-1474.

41. Radjenović, J.; Petrović, M.; Barceló, D., Fate and distribution of pharmaceuticals in wastewater and sewage sludge of the conventional activated sludge (CAS) and advanced membrane bioreactor (MBR) treatment. *Water research* **2009,** *43* (3), 831-841.

42. Ulubay, M.; Yurt, K. K.; Kaplan, A. A.; Atilla, M. K., The use of diclofenac sodium in urological practice: a structural and neurochemical based review. *Journal of Chemical Neuroanatomy* **2018,** *87*, 32-36.

43. Bravo, S. A.; Lamas, M. C.; Salomón, C. J., In-vitro studies of diclofenac sodium controlled-release from biopolymeric hydrophilic matrices. *J Pharm Pharm Sci* **2002,** *5* (3), 213-219.

44. Lonappan, L.; Brar, S. K.; Das, R. K.; Verma, M.; Surampalli, R. Y., Diclofenac and its transformation products: environmental occurrence and toxicity-a review. *Environment International* **2016,** *96*, 127-138.

45. Bagal, M. V.; Gogate, P. R., Degradation of diclofenac sodium using combined processes based on hydrodynamic cavitation and heterogeneous photocatalysis. *Ultrasonics sonochemistry* **2014,** *21* (3), 1035-1043.

46. Sathishkumar, P.; Meena, R. A. A.; Palanisami, T.; Ashokkumar, V.; Palvannan, T.; Gu, F. L., Occurrence, interactive effects and ecological risk of diclofenac in environmental compartments and biota-a review. *Science of The Total Environment* **2020,** *698*, 134057.

47. Maia, G. S.; de Andrade, J. R.; da Silva, M. G.; Vieira, M. G., Adsorption of diclofenac sodium onto commercial organoclay: kinetic, equilibrium and thermodynamic study. *Powder Technology* **2019,** *345*, 140-150.

48. Bhadra, B. N.; Seo, P. W.; Jhung, S. H., Adsorption of diclofenac sodium from water using oxidized activated carbon. *Chemical Engineering Journal* **2016,** *301*, 27-34.

49. Jauris, I.; Matos, C.; Saucier, C.; Lima, E.; Zarbin, A.; Fagan, S.; Machado, F.; Zanella, I., Adsorption of sodium diclofenac on graphene: a combined experimental and theoretical study. *Physical Chemistry Chemical Physics* **2016,** *18* (3), 1526-1536.

50. Vedenyapina, M.; Borisova, D.; Simakova, A.; Proshina, L.; Vedenyapin, A., Adsorption of diclofenac sodium from aqueous solutions on expanded graphite. *Solid Fuel Chemistry* **2013,** *47* (1), 59-63.

51. Sun, Y.-P.; Li, X.-q.; Cao, J.; Zhang, W.-x.; Wang, H. P., Characterization of zero-valent iron nanoparticles. *Advances in colloid and interface science* **2006,** *120* (1-3), 47-56.

52. Dong, H.; Deng, J.; Xie, Y.; Zhang, C.; Jiang, Z.; Cheng, Y.; Hou, K.; Zeng, G., Stabilization of nanoscale zero-valent iron (nZVI) with modified biochar for Cr (VI) removal from aqueous solution. *Journal of Hazardous Materials* **2017,** *332*, 79-86.

53. Jin, Q.; Zhang, S.; Wen, T.; Wang, J.; Gu, P.; Zhao, G.; Wang, X.; Chen, Z.; Hayat, T.; Wang, X., Simultaneous adsorption and oxidative degradation of Bisphenol A by zero-valent iron/iron carbide nanoparticles encapsulated in N-doped carbon matrix. *Environmental Pollution* **2018,** *243*, 218-227.

54. Mortazavian, S.; An, H.; Chun, D.; Moon, J., Activated carbon impregnated by zero-valent iron nanoparticles (AC/nZVI) optimized for simultaneous adsorption and reduction of aqueous hexavalent chromium: Material characterizations and kinetic studies. *Chemical Engineering Journal* **2018,** *353*, 781-795.

55. Wu, Y.; Yue, Q.; Ren, Z.; Gao, B., Immobilization of nanoscale zero-valent iron particles (nZVI) with synthesized activated carbon for the adsorption and degradation of Chloramphenicol (CAP). *Journal of Molecular Liquids* **2018,** *262*, 19-28.

56. Wang, C.; Luo, H.; Zhang, Z.; Wu, Y.; Zhang, J.; Chen, S., Removal of As (III) and As (V) from aqueous solutions using nanoscale zero valent iron-reduced graphite oxide modified composites. *Journal of Hazardous materials* **2014,** *268*, 124-131.

57. Liu, Y.; Sohi, S. P.; Liu, S.; Guan, J.; Zhou, J.; Chen, J., Adsorption and reductive degradation of Cr (VI) and TCE by a simply synthesized zero valent iron magnetic biochar. *Journal of environmental management* **2019,** *235*, 276-281.

58. Chen, B.; Chen, Z.; Lv, S., A novel magnetic biochar efficiently sorbs organic pollutants and phosphate. *Bioresource technology* **2011,** *102* (2), 716-723.

59. Prabu, D.; Parthiban, R.; Senthil Kumar, P.; Kumari, N.; Saikia, P., Adsorption of copper ions onto nano-scale zero-valent iron impregnated cashew nut shell. *Desalination and water treatment* **2016,** *57* (14), 6487-6502.

60. Vimonses, V.; Lei, S.; Jin, B.; Chow, C. W.; Saint, C., Kinetic study and equilibrium isotherm analysis of Congo Red adsorption by clay materials. *Chemical Engineering Journal* **2009,** *148* (2-3), 354-364.

61. Kamel, M.; Youssef, B.; Kamel, M. M., Adsorption of anionic dyes by kaolinites. *Dyes and pigments* **1991,** *15* (3), 175-182.

62. Sarma, G.; Sen Gupta, S.; Bhattacharyya, K., Removal of hazardous basic dyes from aqueous solution by adsorption onto kaolinite and acid-treated kaolinite: kinetics, isotherm and mechanistic study. *SN Applied Sciences* **2019,** *1* (3), 1-15.

63. Alkan, M.; Demirbaş, Ö.; Doğan, M., Adsorption kinetics and thermodynamics of an anionic dye onto sepiolite. *Microporous and mesoporous materials* **2007,** *101* (3), 388-396.

64. Chaari, I.; Fakhfakh, E.; Medhioub, M.; Jamoussi, F., Comparative study on adsorption of cationic and anionic dyes by smectite rich natural clays. *Journal of Molecular Structure* **2019,** *1179*, 672-677.

65. Fabryanty, R.; Valencia, C.; Soetaredjo, F. E.; Putro, J. N.; Santoso, S. P.; Kurniawan, A.; Ju, Y.-H.; Ismadji, S., Removal of crystal violet dye by adsorption using bentonite–alginate composite. *Journal of Environmental Chemical Engineering* **2017,** *5* (6), 5677-5687.

66. Derakhshani, E.; Naghizadeh, A., Optimization of humic acid removal by adsorption onto bentonite and montmorillonite nanoparticles. *Journal of Molecular Liquids* **2018,** *259*, 76-81.

67. Halim, A. A.; Aziz, H. A.; Johari, M. A. M.; Ariffin, K. S., Comparison study of ammonia and COD adsorption on zeolite, activated carbon and composite materials in landfill leachate treatment. *Desalination* **2010,** *262* (1-3), 31-35.

68. Ezzatahmadi, N.; Ayoko, G. A.; Millar, G. J.; Speight, R.; Yan, C.; Li, J.; Li, S.; Zhu, J.; Xi, Y., Clay-supported nanoscale zero-valent iron composite materials for the remediation of contaminated aqueous solutions: a review. *Chemical engineering journal* **2017,** *312*, 336-350.

69. https://pencils.com/pages/hb-graphite-grading-scale.

70. Sousa, M. C.; Buchanan, J. W. In *Observational models of graphite pencil materials*, Computer Graphics Forum, Wiley Online Library: 2000; pp 27-49.

71. Foster, C. W.; Brownson, D. A.; de Souza, A. P. R.; Bernalte, E.; Iniesta, J.; Bertotti, M.; Banks, C. E., Pencil it in: pencil drawn electrochemical sensing platforms. *Analyst* **2016,** *141* (13), 4055-4064.

72. Tavares, P. H. C. P.; Barbeira, P. J. S., Influence of pencil lead hardness on voltammetric response of graphite reinforcement carbon electrodes. *Journal of Applied Electrochemistry* **2008,** *38* (6), 827-832.

73. David, I. G.; Popa, D.-E.; Buleandra, M., Pencil graphite electrodes: a versatile tool in electroanalysis. *Journal of analytical methods in chemistry* **2017,** *2017*.

74. Wang, J.; Kawde, A.-N.; Sahlin, E., Renewable pencil electrodes for highly sensitive stripping potentiometric measurements of DNA and RNA. *Analyst* **2000,** *125* (1), 5-7.

75. Chen, Z.-x.; Jin, X.-y.; Chen, Z.; Megharaj, M.; Naidu, R., Removal of methyl orange from aqueous solution using bentonite-supported nanoscale zero-valent iron. *Journal of colloid and interface science* **2011,** *363* (2), 601-607.

76. Lin, D.; Hu, L.; Lo, I.; Yu, Z., Size distribution and phosphate removal capacity of nano zero-valent iron (nZVI): Influence of pH and ionic strength. *Water* **2020,** *12* (10), 2939.

77. Sawafta, R.; Shahwan, T., A comparative study of the removal of methylene blue by iron nanoparticles from water and water-ethanol solutions. *Journal of Molecular Liquids* **2019,** *273*, 274-281.

78. Murray, H. H.; Johnson, H. M., Pencil clays. Google Patents: 1961.

79. Liu, A.; Liu, J.; Zhang, W.-x., Transformation and composition evolution of nanoscale zero valent iron (nZVI) synthesized by borohydride reduction in static water. *Chemosphere* **2015,** *119*, 1068-1074.

80. Skrzypczynska, K.; Kusmierek, K.; Swiatkowski, A.; Dabek, L., The influence of pencil graphite hardness on voltammetric detection of pentachlorophenol. *Int. J. Electrochem. Sci* **2018,** *13*, 88-100.

81. Xu, C.; Yang, W.; Liu, W.; Sun, H.; Jiao, C.; Lin, A.-j., Performance and mechanism of Cr (VI) removal by zero-valent iron loaded onto expanded graphite. *Journal of Environmental Sciences* **2018,** *67*, 14-22.

82. Ramachandran, E.; Ramukutty, S., Growth, morphology, spectral and thermal studies of gel grown diclofenac acid crystals. *Journal of crystal growth* **2014,** *389*, 78-82.

83. Rončević, S.; Nemet, I.; Ferri, T. Z.; Matković-Čalogović, D., Characterization of nZVI nanoparticles functionalized by EDTA and dipicolinic acid: A comparative study of metal ion removal from aqueous solutions. *RSC advances* **2019,** *9* (53), 31043-31051.

84. Largitte, L.; Lodewyckx, P., Kinetics and thermodynamics of the adsorption of lead (II) on a activated carbon from coconut shells. *Eurasian Chemico-Technological Journal* **2013,** *15* (4), 283-292.

85. Antunes, M.; Esteves, V. I.; Guégan, R.; Crespo, J. S.; Fernandes, A. N.; Giovanela, M., Removal of diclofenac sodium from aqueous solution by Isabel grape bagasse. *Chemical Engineering Journal* **2012,** *192*, 114-121.

86. Simonin, J.-P., On the comparison of pseudo-first order and pseudo-second order rate laws in the modeling of adsorption kinetics. *Chemical Engineering Journal* **2016,** *300*, 254-263.

87. Vijayakumar, G.; Tamilarasan, R.; Dharmendirakumar, M., Adsorption, Kinetic, Equilibrium and Thermodynamic studies on the removal of basic dye Rhodamine-B from aqueous solution by the use of natural adsorbent perlite. *J. Mater. Environ. Sci* **2012,** *3* (1), 157-170.

88. Rout, S.; Kumar, A.; Ravi, P. M.; Tripathi, R. M., Pseudo second order kinetic model for the sorption of U (VI) onto soil: A comparison of linear and non-linear methods. *International Journal of Environmental Sciences* **2015,** *6* (1), 145.

89. Shahwan, T., Sorption kinetics: obtaining a pseudo-second order rate equation based on a mass balance approach. *Journal of Environmental Chemical Engineering* **2014,** *2* (2), 1001-1006.

90. Radnia, H.; Ghoreyshi, A. A.; Younesi, H.; Najafpour, G. D., Adsorption of Fe (II) ions from aqueous phase by chitosan adsorbent: equilibrium, kinetic, and thermodynamic studies. *Desalination and Water Treatment* **2012,** *50* (1-3), 348-359.

91. Afshin, S.; Rashtbari, Y.; Shirmardi, M.; Vosoughi, M.; Hamzehzadeh, A., Adsorption of Basic Violet 16 dye from aqueous solution onto mucilaginous seeds of Salvia sclarea: kinetics and isotherms studies. *Desalination and water treatment* **2019,** *161*, 365-375.

92. Thilagan, J.; Gopalakrishnan, S.; Kannadasan, T., A comparative study on adsorption of copper (ii) ions in aqueous solution by;(a) chitosan blended with cellulose and cross linked by formaldehyde,(b) chitosan immobilised on red soil,(c) chitosan reinforced by banana stem fibre. *Int. J. Appl. Eng. Technol.* **2013,** *3* (1), 35-60.

93. Zhao, G.; Li, J.; Ren, X.; Chen, C.; Wang, X., Few-layered graphene oxide nanosheets as superior sorbents for heavy metal ion pollution management. *Environmental science & technology* **2011,** *45* (24), 10454-10462.

94. Sulaiman, S. M.; Al-Jabari, M. H., Enhanced adsorptive removal of diclofenac sodium from aqueous solution by bentonite-supported nanoscale zero-valent iron. *Arab Journal of Basic and Applied Sciences* **2021,** *28* (1), 51-63.

95. Boruah, P. K.; Sharma, B.; Hussain, N.; Das, M. R., Magnetically recoverable Fe3O4/graphene nanocomposite towards efficient removal of triazine pesticides from aqueous solution: Investigation of the adsorption phenomenon and specific ion effect. *Chemosphere* **2017,** *168*, 1058-1067.

96. Cottet, L.; Almeida, C.; Naidek, N.; Viante, M.; Lopes, M.; Debacher, N., Adsorption characteristics of montmorillonite clay modified with iron oxide with respect to methylene blue in aqueous media. *Applied Clay Science* **2014,** *95*, 25-31.

97. Espenson, J. H., *Chemical kinetics and reaction mechanisms*. Citeseer: 1995; Vol. 102.

98. Atkins, P.; Atkins, P. W.; de Paula, J., *Atkins' physical chemistry*. Oxford university press: 2014.

99. Shahwan, T., Critical insights into the limitations and interpretations of the determination ofΔ Go,Δ Ho, andΔ So of sorption of aqueous pollutants on different sorbents. *Colloid and Interface Science Communications* **2021,** *41*, 100369.

100. Husein, D. Z.; Hassanien, R.; Al-Hakkani, M. F., Green-synthesized copper nano-adsorbent for the removal of pharmaceutical pollutants from real wastewater samples. *Heliyon* **2019,** *5* (8), e02339.

101. Húmpola, P.; Odetti, H.; Fertitta, A. E.; Vicente, J. L., Thermodynamic analysis of adsorption models of phenol in liquid phase on different activated carbons. *Journal of the Chilean Chemical Society* **2013,** *58* (1), 1541-1544.

102. Yu, Y.; Zhuang, Y.-Y.; Wang, Z.-H., Adsorption of water-soluble dye onto functionalized resin. *Journal of colloid and interface science* **2001,** *242* (2), 288-293.

Appendix

Diclofenac Sodium calibration curve